R-04-46

Local-scale modelling of density-driven flow for the phases of repository operation and post-closure at Beberg

O Jaquet, P Siegel
Colenco Power Engineering Ltd

September 2004

Svensk Kärnbränslehantering AB
Swedish Nuclear Fuel
and Waste Management Co
Box 5864
SE-102 40 Stockholm Sweden
Tel 08-459 84 00
+46 8 459 84 00
Fax 08-661 57 19
+46 8 661 57 19

ISSN 1402-3091
SKB Rapport R-04-46

Local-scale modelling of density-driven flow for the phases of repository operation and post-closure at Beberg

O Jaquet, P Siegel
Colenco Power Engineering Ltd

September 2004

Contents

1 Introduction

SKB has carried out modelling studies at local scale for Beberg. In comparison to previous studies, the newly developed model includes the repository. In particular, it was the effects of density-driven flow and the role of discrete fractures which were analysed for the operation and post-closure phases of the repository.

The numerical modelling task was performed using CONNECTFLOW, which allows the use of discrete and continuum approaches.

2 Objectives

The objectives of the study are based on technical specifications established by SKB and can be summarised as follows:

- Evaluation of the up-coning of saltwater for the phase of repository operation.
- Estimation of the time scale for the “re-saturation“ phase after repository closure.
- Assessment of the feasibility of performing CONNECTFLOW simulations at a local scale with a repository under atmospheric pressure conditions.

The report begins with an account of the modelling approach applied. Then, the results of the different cases simulated are described, analysed and interpreted in detail. Finally, conclusions are drawn up together with some recommendations related to potential modelling issues for the future.

3 Modelling approach

The approach followed for the hydrogeological modelling of Beberg takes into account two embedded scales: a local scale at which the granitic medium is considered as a continuum and a repository scale, where the medium is fractured and therefore regarded to be discrete. For the purpose of modelling density-driven flow at both scales, the following steps were undertaken:

1. Modelling fracture networks at the repository scale.
2. Modelling flow in the fracture networks at the repository scale for the upscaling of hydraulic properties to a continuum at local scale.
3. Modelling density-driven flow at local scale for the operation and post-closure phases of the repository.

The modelling approach is discussed in terms of phenomenology, parameters and boundary conditions considered. This study relies on previous work performed by /Hartley et al, 1998/, /Gylling et al, 1999/, /Marsic et al, 2000/, /Marsic et al, 2001/, /Marsic et al, 2002/ and /Gylling et al, 2003/.

3.1 Location and dimension

Beberg is modelled after the Finnsjön site of Northern Uppland located in Central Sweden. The developed model comprises local and repository scales which correspond to the following embedded domains (see Figure 3-1):

- Local domain: the size of the local domain is 8,000 x 8,000 x 1,500 m (length x width x depth).
- Repository domain: the repository domain lies within the local domain at a depth of 320 to 500 m. The size of the repository domain is 1,600 x 1,200 x 180 m (length x width x depth).

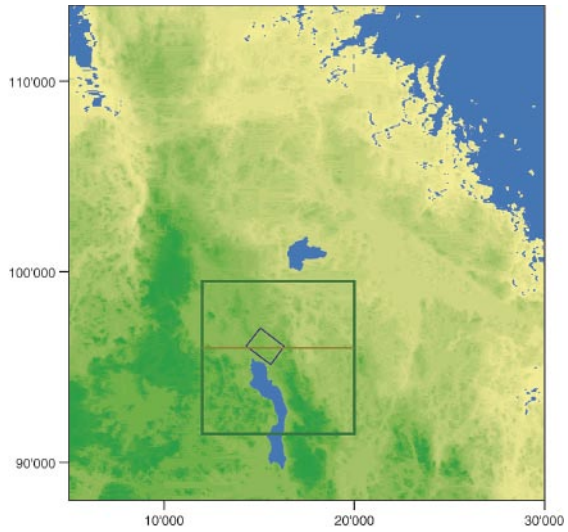

Figure 3-1. *Modelling scales: local (green square) and repository (blue rectangle) domains; cut for 2D model (orange line).*

3.2 Fracture zones

About forty fracture zones of kilometric extent were considered within the borders of the local-scale model. Their locations are shown in Figure 3-2. Each fracture zone intersects the total thickness of the domain and has a specified width and orientation.

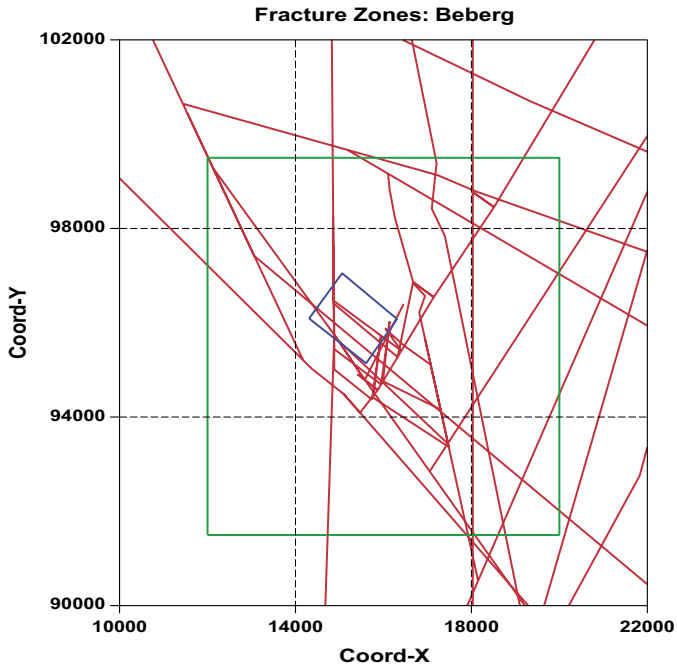

Figure 3-2. *Location of fracture zones (red) for Beberg with respect to the local (green) and repository (blue) domains.*

3.3 Fractures

At the repository scale, fractures from deka- to hectometric size were taken into account. At that scale, the complexity of the granitic medium precludes the exact knowledge of the geometric and hydraulic properties of each fracture. Therefore, the properties of the fracture network at repository scale were derived using a stochastic approach.

3.4 Repository

The repository lies between 400 and 420 m below sea level. Two variants were considered for the model representation:

- Variant I: simplified layout as a slab.
- Variant II: layout honouring the tunnel system.

Based on SKB specifications, both variants are represented with a uniform thickness of 20 m. The southern (small) part of the repository was disregarded.

3.5 Phenomenology

Local model

The density-driven flow as induced by the variable salinity of the groundwater is expressed in terms of flow and transport equations. The following forms (implemented in NAMMU) were applied – fully coupled /Cliffe et al, 1998/ – for the modelling at local scale.

The flow equations are governed by Darcy's law:

$$\mathbf{q} = -\frac{\mathbf{k}}{\mu}\left(\nabla p^R - (\rho - \rho_0)\mathbf{g}\right) \tag{1}$$

where:

$\mathbf{q}$: Darcy velocity

$\mathbf{k}$: intrinsic permeability tensor

μ: fluid viscosity

p^R: residual pressure with $p^R = p+\rho_0\mathbf{g}(z-z_o)$

p: pressure

ρ: fluid density

ρ_0: reference density of fluid (freshwater)

z: elevation

z_0: reference elevation

$\mathbf{g}$: gravitational acceleration

and the continuity equation:

$$\frac{\partial}{\partial t}(\varphi\rho) + \nabla \cdot (\rho \mathbf{q}) = 0 \tag{2}$$

where:

φ: total porosity.

Using the specific storage coefficient:

$$S = \rho \mathbf{g}\left(\frac{\partial \varphi}{\partial p} + \beta\varphi\right) \tag{3}$$

where:

S: specific storage coefficient

ß: fluid compressibility

the continuity equation becomes:

$$\frac{S}{\mathbf{g}}\frac{\partial p^R}{\partial t} + \nabla \cdot (\rho \mathbf{q}) + \varphi \frac{\partial \rho}{\partial c}\frac{\partial c}{\partial t} = 0 \tag{4}$$

where:

c: concentration of solute as a mass fraction of the reference concentration.

By combining equations (2) and (4), the continuity equation can be written as:

$$\frac{\partial}{\partial t}(\varphi\rho) = \frac{S}{\mathbf{g}}\frac{\partial p^R}{\partial t} + \varphi \frac{\partial \rho}{\partial c}\frac{\partial c}{\partial t} \tag{5}$$

Regarding salt transport, the advection-dispersion equation implies:

$$\frac{\partial}{\partial t}(\varphi\rho c) + \nabla \cdot (\rho \mathbf{q} c) = \nabla \cdot (\varphi\rho \underline{\underline{D}} \cdot \nabla c) \tag{6}$$

where:

$\underline{\underline{D}}$: hydrodynamic dispersion tensor.

The hydrodynamic dispersion tensor is defined as follows:

$$\underline{\underline{D}} = \frac{D_m}{\tau}\delta_{ij} + \alpha_T v \delta_{ij} + (\alpha_L - \alpha_T)\frac{v_i v_j}{v} \tag{7}$$

where:

D_m: molecular diffusion coefficient

τ: tortuosity

α_L, α_T: transverse and longitudinal dispersivity

$\mathbf{v}$: porewater velocity (with $\mathbf{v} = \frac{\mathbf{q}}{\phi}$ and $v = \sqrt{\mathbf{v} \cdot \mathbf{v}}$).

The dependence of density upon the solute concentration is given by the following equation of state:

$$\rho = \left(\frac{1 - c}{\rho_0} + \frac{c}{\rho_s} \right)^{-1} \tag{8}$$

where:

ρ_s: saturation density of the fluid.

The salinity can be expressed as a function of density using the following equation /Svensson, 1999/:

$$s = \frac{\rho - \rho_0}{\rho_0 \, a} \tag{9}$$

where:

s: salinity

a: coefficient (= $7.41 \cdot 10^{-3}$).

All calculations were performed under saturated conditions (repository included); i.e. two-phase flow effects in the vicinity of the repository are neglected. No free surface is taken into account at this stage in the upper part of the model.

Repository model

For the repository-model calculations, flow is described in the 2D plane of each fracture of the network. The flow in each fracture is represented by the "effective parallel plate model" corresponding to a single equivalent transmissivity. The flux is obtained using the linear relation derived from a consideration of Poiseuille applied to slow flow through a planar fracture of constant aperture /Grinrod et al, 1991/. Within CONNECTFLOW, the finite-element method is applied to model steady-state flow in each discretised fracture by solving the continuity equation where the flux is of Poiseuille type.

3.6 Hydraulic and geometric parameters

For the modelling at Beberg, the hydraulic properties of the rock mass, and the geometric and hydraulic parameters of the fracture zones (i.e. discontinuities at kilometric scale) and the fractures (i.e. discontinuities from deka- to hectometric scale) are given in Tables 3-1 to 3-8.

The hydraulic conductivity of the rock mass was assumed to follow a log-normal distribution. An exponential variogram with an isotropic correlation length of 150 m (i.e. a practical range of 450 m) was applied for the stochastic simulation of the hydraulic conductivity. The hydraulic conductivity of the rock mass was considered as a scalar before the upscaling of the fracture zone was performed with the IFZ (Implicit Fracture Zone) method.

Table 3-1. Hydraulic parameters of the rock mass (after values for intermediate scale from Table 4-1 in /Marsic et al, 2002/).

Depth (m)	Geometric mean of hydraulic conductivity (m/s)	Standard deviation (log 10)	Correlation length (m)	Specific storage (m^{-1})
0–35	$1.6 \cdot 10^{-7}$	0.46	150	$1.2 \cdot 10^{-6}$
35–875	$1.3 \cdot 10^{-8}$	0.32	150	$1.2 \cdot 10^{-6}$
875–1,500	$5.0 \cdot 10^{-9}$	0.32	150	$1.2 \cdot 10^{-6}$

The value for the specific storage was obtained using the following expression applied to granitic rocks:

$$S = \rho \mathbf{g}(\varphi\beta+\alpha) \quad (10)$$

where:

S: specific storage

α: porous medium compressibility.

with:

$$\alpha = \frac{3(1 - 2\nu)}{E}$$

where:

ν: Poisson ratio (= 0.2; after /Rhén et al, 1997/)

E: deformation modulus (= $1.6 \cdot 10^{+10}$ Pa; after /Rhén et al, 1997/).

At the local scale, the fracture zones were described deterministically in terms of geometry and flow parameters (see Table 3-2). At the repository scale, the description of the fractures requires a stochastic approach where the parameters were defined using statistical distributions. The shape of the fractures was assumed to be rectangular. Six sets of fractures with specific parameters were defined and referred to as “green fractures, sets 1 to 3” and “red fractures, sets 1 to 3”. Their parameters (see Tables 3-3 to 3-8) were taken from the Aberg site using data from /Dershowitz et al, 1999/ and scaled to Beberg /Gylling et al, 2003/.

Table 3-2. Hydraulic and geometric parameters of fracture zones (local scale).

Number of fracture zones	$K_{fracture\ zone}$ ($m \cdot s^{-1}$)	Width (m)
40	$1.0 \cdot 10^{-9}$–$1.7 \cdot 10^{-4}$	20–100

Table 3-3. Green fractures, set 1: hydraulic and geometric parameters (repository scale).

Parameter	Distribution	Mean	Std. deviation	Dispersion	Minimum	Maximum
Areal density (m^2/m^3)	Poisson	**0.017**	–	–	–	–
Length_1 ln (m)	Log-normal	3.000 (20 m)	0.788	–	3.680	7.600 (2000 m)
Length_2 ln (m)	Log-normal	3.000	0.788	–	3.680	7.600
Dip azimuth (°)	Fisher	**51.0**	–	–	–	–
Dip angle (°)	Fisher	**2.0**	–	**1.0**	–	–
Transmissivity ln ($m^2 \cdot s^{-1}$)	Log-normal	–15.6520	1.8600	–	–20.7233	–7.0000

Table 3-4. Green fractures, set 2: hydraulic and geometric parameters (repository scale).

Parameter	Distribution	Mean	Std. deviation	Dispersion	Minimum	Maximum
Areal density (m^2/m^3)	Poisson	**0.011**	–	–	–	–
Length_1 ln (m)	Log-normal	3.000	0.788	–	3.680	7.600
Length_2 ln (m)	Log-normal	3.000	0.788	–	3.680	7.600
Dip azimuth (°)	Fisher	**148.0**	–	–	–	–
Dip angle (°)	Fisher	**14.0**	–	**8.9**	–	–
Transmissivity ln ($m^2 \cdot s^{-1}$)	Log-normal	–15.6520	1.8600	–	–20.7233	–7.0000

Table 3-5. Green fractures, set 3: hydraulic and geometric parameters (repository scale).

Parameter	Distribution	Mean	Std. deviation	Dispersion	Minimum	Maximum
Areal density (m^2/m^3)	Poisson	**0.010**	–	–	–	–
Length_1 ln (m)	Log-normal	3.000	0.788	–	3.680	7.600
Length_2 ln (m)	Log-normal	3.000	0.788	–	3.680	7.600
Dip azimuth (°)	Fisher	**31.0**	–	–	–	–
Dip angle (°)	Fisher	**87.0**	–	**18**	–	–
Transmissivity ln ($m^2 \cdot s^{-1}$)	Log-normal	–15.6520	1.8600	–	–20.7233	–7.0000

Table 3-6. Red fractures, set 1: hydraulic and geometric parameters (repository scale).

Parameter	Distribution	Mean	Std. deviation	Dispersion	Minimum	Maximum
Areal density (m^2/m^3)	Poisson	**0.0875**	–	–	–	–
Length_1 ln (m)	Log-normal	2.373 (11 m)	0.472	–	–0.916	3.689 (40 m)
Length_2 ln (m)	Log-normal	2.373	0.472	–	–0.916	3.689
Dip azimuth (°)	Fisher	**51.0**	–	–	–	–
Dip angle (°)	Fisher	**2.0**	–	**1.0**	–	–
Transmissivity ln ($m^2 \cdot s^{-1}$)	Log-normal	–15.6520	1.8600	–	–20.7233	–7.0000

Table 3-7. Red fractures, set 2: hydraulic and geometric parameters (repository scale).

Parameter	Distribution	Mean	Std. deviation	Dispersion	Minimum	Maximum
Areal density (m^2/m^3)	Poisson	**0.0575**	–	–	–	–
Length_1 ln (m)	Log-normal	2.373	0.472	–	–0.916	3.689
Length_2 ln (m)	Log-normal	2.373	0.472	–	–0.916	3.689
Dip azimuth (°)	Fisher	**148.0**	–	–	–	–
Dip angle (°)	Fisher	**14.0**	–	**8.9**	–	–
Transmissivity ln ($m^2 \cdot s^{-1}$)	Log-normal	–15.6520	1.8600	–	–20.7233	–7.0000

Table 3-8. Red fractures, set 3: hydraulic and geometric parameters (repository scale).

Parameter	Distribution	Mean	Std. deviation	Dispersion	Minimum	Maximum
Areal density (m^2/m^3)	Poisson	**0.0550**	–	–	–	–
Length_1 ln (m)	Log-normal	2.373	0.472	–	–0.916	3.689
Length_2 ln (m)	Log-normal	2.373	0.472	–	–0.916	3.689
Dip azimuth (°)	Fisher	**31.0**	–	–	–	–
Dip angle (°)	Fisher	**87.0**	–	**18**	–	–
Transmissivity ln ($m^2 \cdot s^{-1}$)	Log-normal	–15.6520	1.8600	–	–20.7233	–7.000

In the local model, the slab or the tunnels representing the repository were backfilled completely during the phase of resaturation (i.e. repository post-closure). The repository was assumed to be homogeneous with respect to its material properties and, at this stage, no skin around the tunnels/repository was taken into account. Two values were considered for the hydraulic conductivity of the backfill (see Table 3-9).

Table 3-9. Hydraulic parameters for the repository.

Depth (m)	$K_{backfill}$ (reference) (m/s)	$K_{backfill}$ (variant) (m/s)	S (m^{-1})
420–400	$1.0 \cdot 10^{-10}$	$1.0 \cdot 10^{-8}$	$1.2 \cdot 10^{-6}$

3.7 Transport parameters

The transport parameters for the rock mass are given in Table 3-10. For the fracture zones a total porosity of 5% /Marsic et al, 2002/ was applied.

Table 3-10. Transport parameters for the rock mass (after values for intermediate scale of Table 4-2 from /Marsic et al, 2002/).

Depth (m)	Porosity (total) (–)	α_L (m)	α_T (m)	Molecular diffusion coefficient (m^2/s)
0–35	$2 \cdot 10^{-2}$	60	30	$3.0 \cdot 10^{-9}$
35–875	$2 \cdot 10^{-2}$	60	30	$3.0 \cdot 10^{-9}$
> 875	$2 \cdot 10^{-2}$	60	30	$3.0 \cdot 10^{-9}$

The transport parameters for the repository are given in Table 3-11.

Table 3-11. Transport parameters for the repository.

$Porosity_{backfill}$(total) (–)	α_L (m)	α_T (m)	Molecular diffusion coefficient (m^2/s)
0.35	30	15	$3.0 \cdot 10^{-9}$

3.8 Finite-element meshes

For the local model, the discretisation was performed using a finite-element mesh with cuboid elements (8 nodes) of non-uniform size (see Table 3-12). The repository was also discretised using cuboid elements of smaller size embedded within the local model (see Figure 3-3).

Table 3-12. Discretisation parameters for the local model.

Element size (m) Local scale	Repository scale	Total number of elements
65	15	490,800

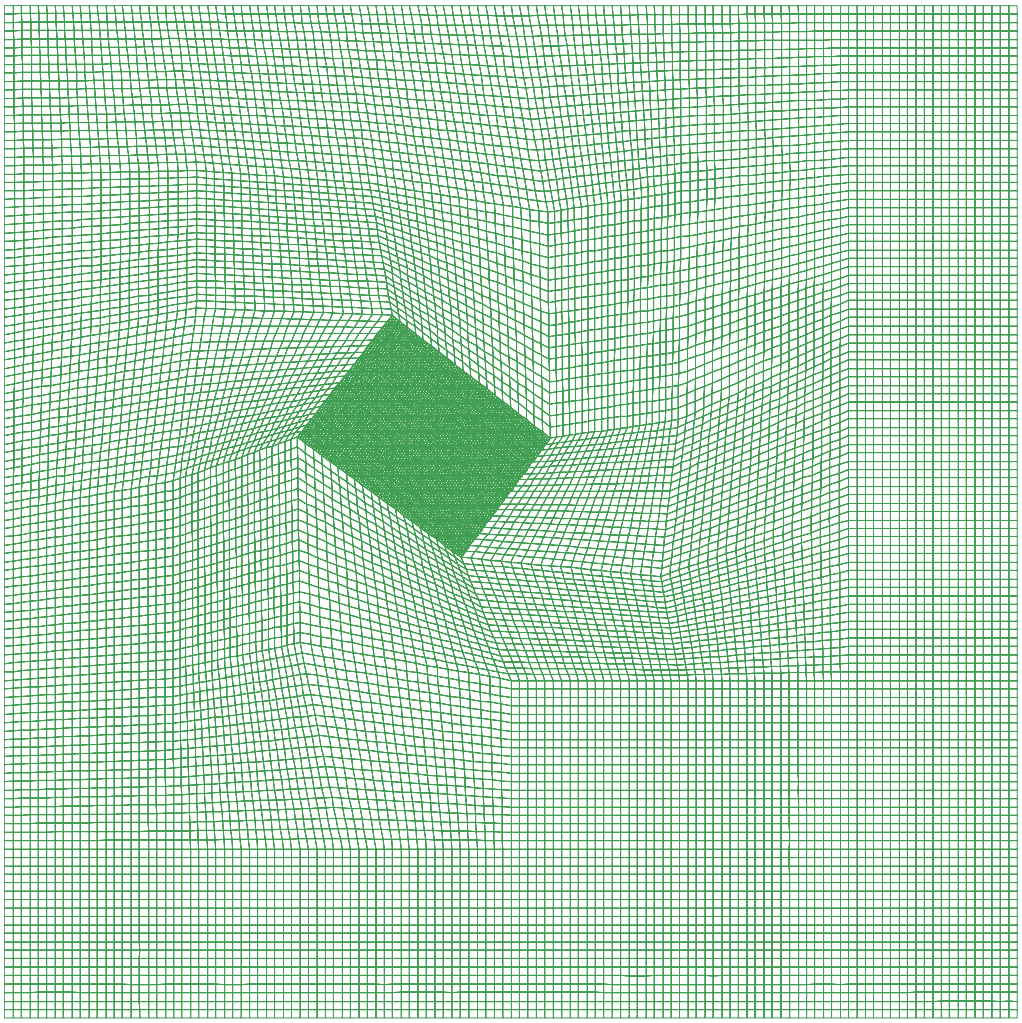

Figure 3-3. *Embedded finite-element mesh with local (8,000 x 8,000 m) and repository (1,600 x 1,200 m) domains.*

Two variants were considered for the repository (see Figure 3-4 and Figure 3-5):

- Variant I (reference case): the repository was simplified as a 3D rectangular slab oriented according to the repository layout.
- Variant II: the transport and deposition tunnels of the repository were explicitly discretised at repository depth. Shafts and access tunnels from the surface were disregarded.

The topography extracted from the SKB-GIS database (with a 50 m resolution) was assigned to the top surface of the finite-element mesh of the local model.

For the repository model, the fractures were discretised using 2D triangular elements. The rock matrix surrounding the fracture network and the repository/tunnels was not considered at that scale.

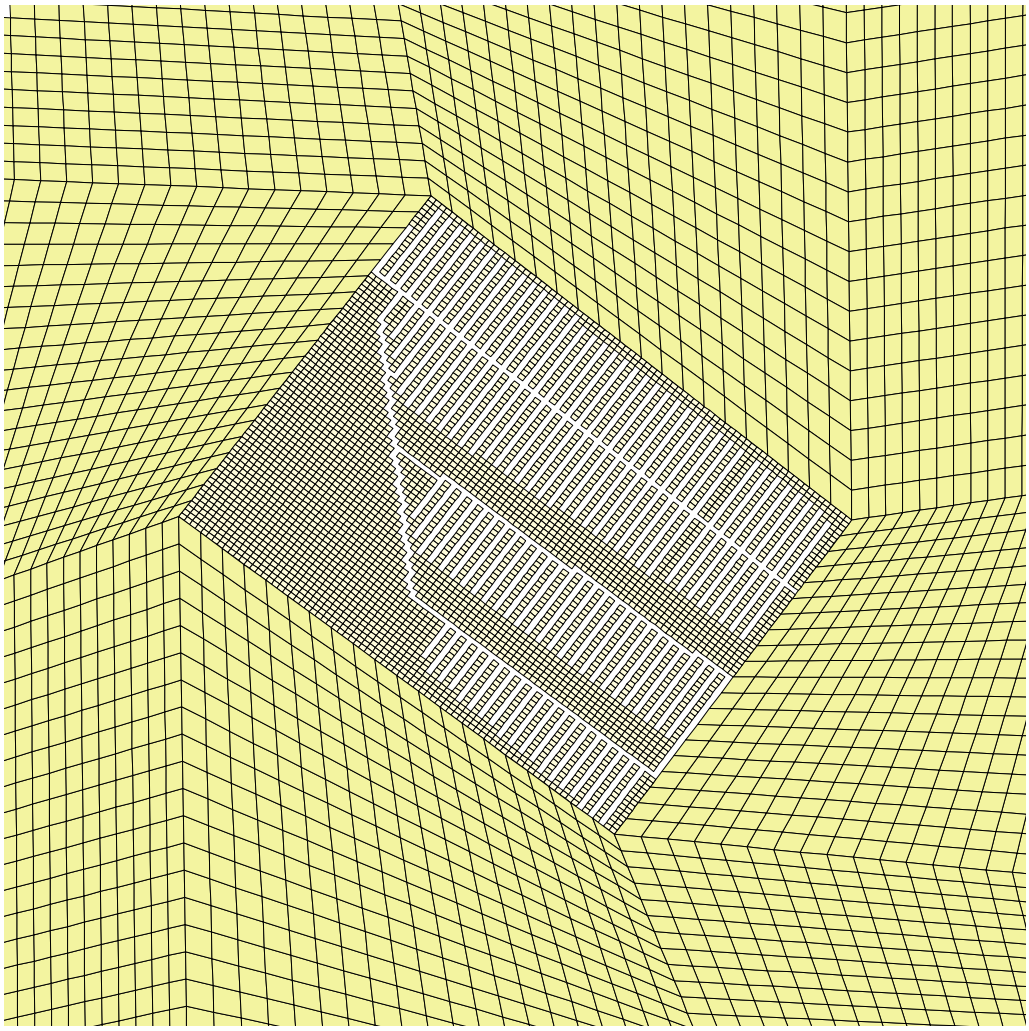

Figure 3-4. *Embedded finite-element mesh (with a mesh reduction factor of 4) with explicit discretisation of repository tunnels.*

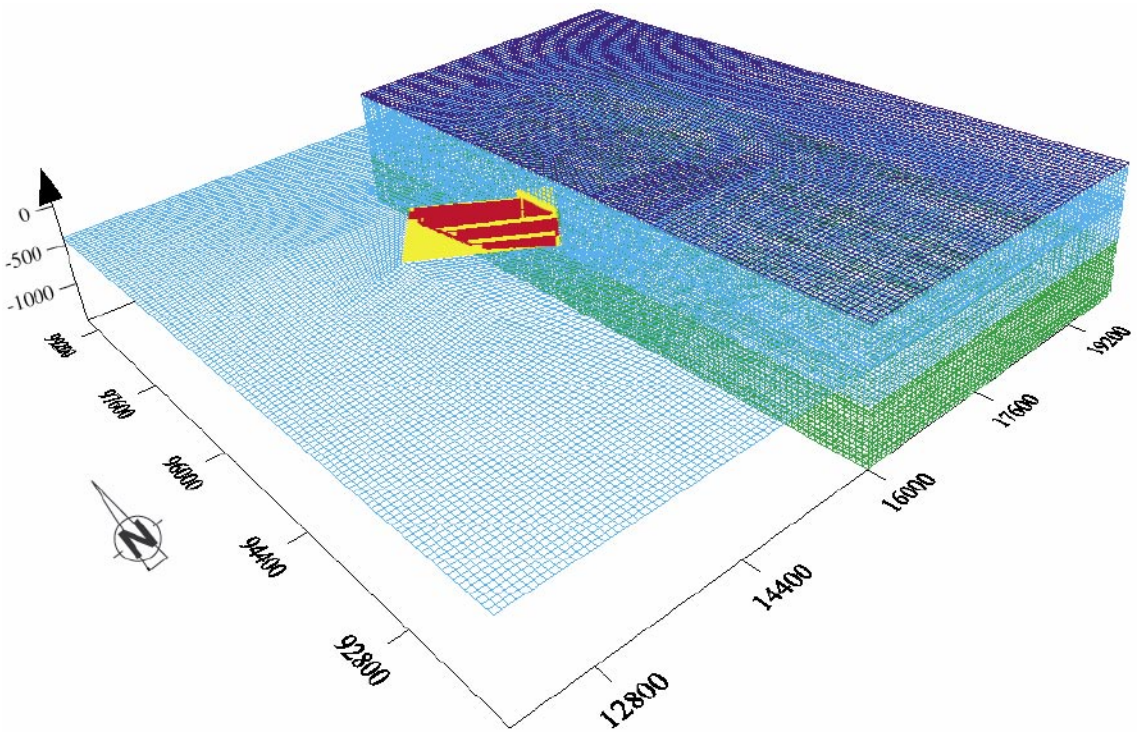

Figure 3-5. *3D finite-element mesh with repository variant I (yellow) and repository variant II (red).*

4 Simulations

The task of modelling the impact of the repository at local scale was divided into four steps:

- Stochastic simulation and upscaling of hydraulic properties from repository scale to local scale.
- Stochastic simulation of hydraulic conductivity at local scale.
- Implicit integration of fracture zones.
- Modelling density-driven flow for the repository phases of operation and post-closure.

The results from these modelling steps are discussed below.

4.1 Stochastic simulation at repository scale and upscaling

The following variants (see Figure 4-1) were considered for the repository layout at local scale (cf Section 3.4):

- Variant I (reference case): simplified layout as a slab surrounded by the repository domain characterised by a single equivalent hydraulic conductivity.
- Variant II : layout honouring the tunnel system surrounded by the repository domain characterised by a spatially variable equivalent hydraulic conductivity.

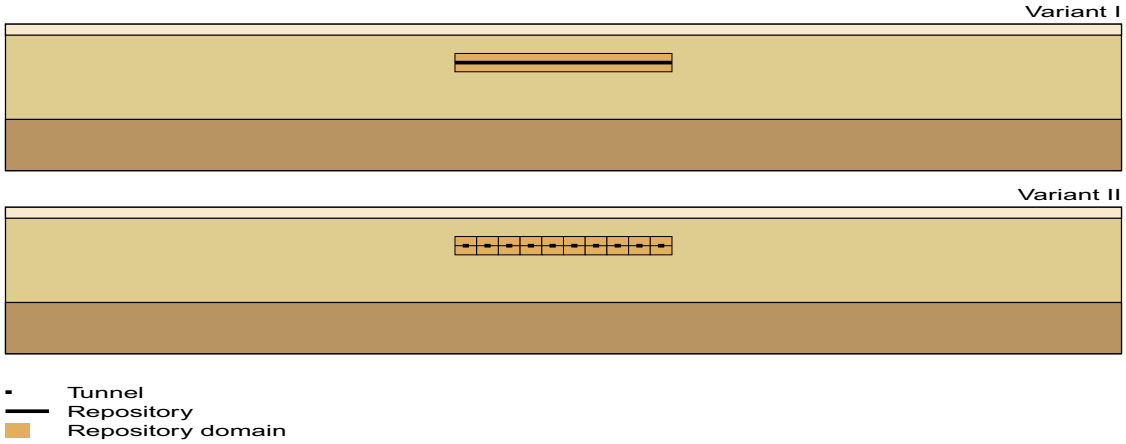

Figure 4-1. *Repository geometry for Variant I with a single equivalent hydraulic conductivity, in the repository domain; and Variant II with spatially variable equivalent hydraulic conductivity, $K_{DFN}(x)$, in the repository domain.*

Equivalent hydraulic conductivity for Variant I

In the reference case, the repository domain was represented by a 3D box (cf Section 3.1) containing the repository slab. At local scale, the repository box was considered as a uniform continuum and, for this purpose, the (discrete) hydraulic properties of the fractures at repository scale were upscaled to a single equivalent hydraulic conductivity at local scale.

At repository scale, the geometric and hydraulic properties of fracture networks were simulated stochastically with CONNECTFLOW using statistical distributions and the parameters (cf Table 3-3 to 3-8) for six sets of fractures. This means that in terms of flow parameters, a transmissivity value was simulated for each fracture. The upscaling of discrete hydraulic conductivity at repository scale to a continuum at local scale was achieved with flow calculations using CONNECTFLOW. Equivalent hydraulic conductivities were calculated for block sizes with increasing scales (see Table 4-1, Figure 4-2 and Figure 4-3).

The results reveal that beyond the scale of 200 m, the variability of the equivalent hydraulic conductivity becomes negligible. This effect is explained when comparing this calculation scale to the mean fracture length (i.e. 20 m and 11 m for the green and the red sets of fractures, respectively). When the scale for the calculation of the equivalent conductivity is large enough with respect to fracture length, then the value of the equivalent hydraulic conductivity becomes less sensitive to small scale variability.

Due to the small differences between the components of the hydraulic permeability tensor, a scalar value equal to $4.0 \cdot 10^{-8}$ m/s was chosen from Table 4-1 for the equivalent hydraulic conductivity of the 3D repository domain for the local model.

This upscaling enables salt calculations to be performed at local scale while including fracture characteristics at repository scale.

Table 4-1. Equivalent hydraulic conductivity for the repository domain.

Block length (m)	K_{11} (m/s)	K_{22} (m/s)	K_{33} (m/s)	Areal density (m^2/m^3)	Number of fractures
100	$3.8 \cdot 10^{-8}$	$5.3 \cdot 10^{-8}$	$3.5 \cdot 10^{-8}$	0.248	1,563
200	$3.1 \cdot 10^{-8}$	$4.3 \cdot 10^{-8}$	$3.0 \cdot 10^{-8}$	0.245	10,878
250	$3.2 \cdot 10^{-8}$	$4.0 \cdot 10^{-8}$	$2.9 \cdot 10^{-8}$	0.238	20,516
300	$3.4 \cdot 10^{-8}$	$4.1 \cdot 10^{-8}$	$3.1 \cdot 10^{-8}$	0.239	34,675

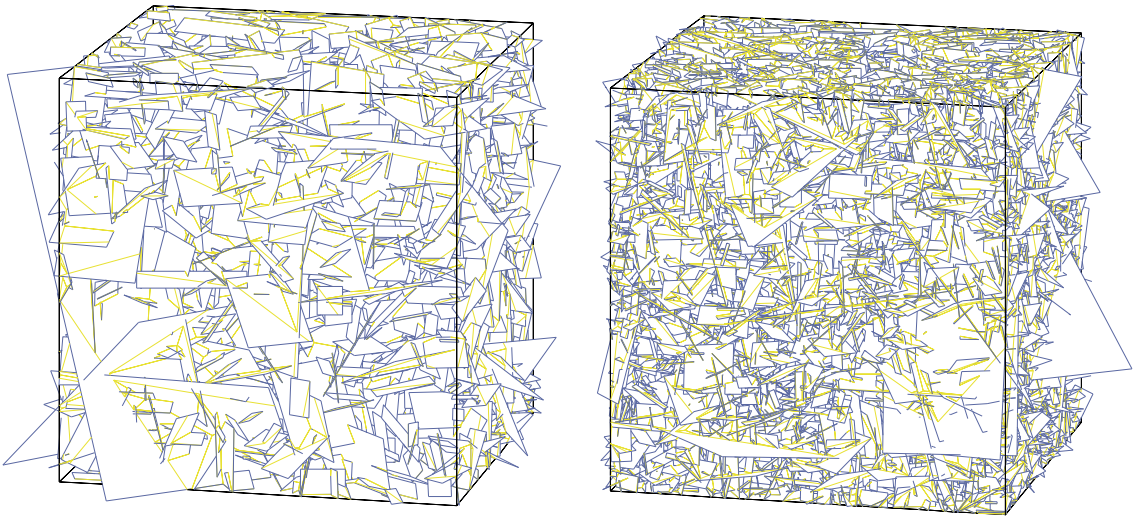

Figure 4-2. *Upscaling from repository scale to local scale (at 100 and 200 m).*

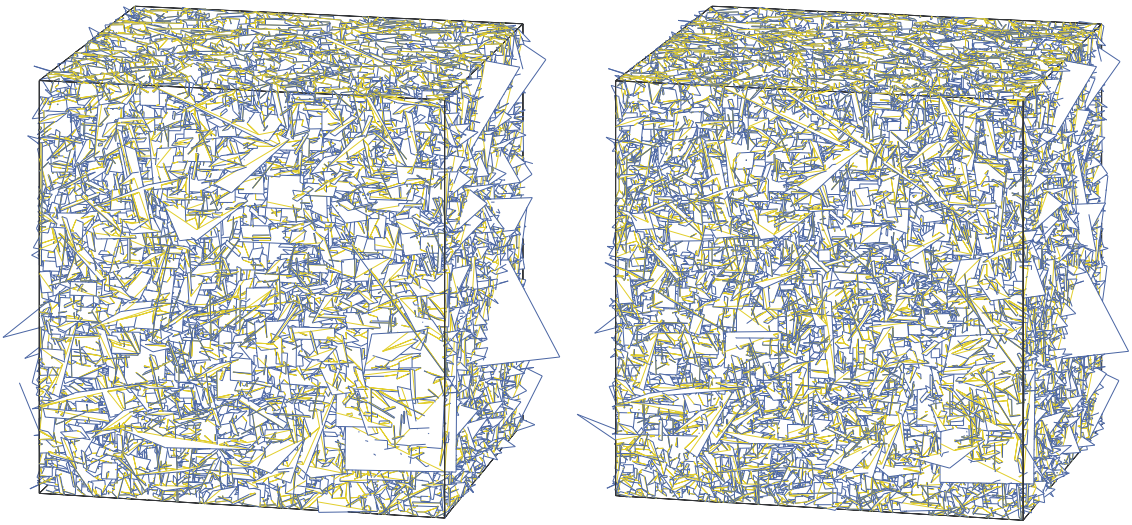

Figure 4-3. *Upscaling from repository scale to local scale (at 250 and 300 m).*

Equivalent hydraulic conductivity for Variant II

For Variant II, the repository domain surrounding the tunnel layout was subdivided into blocks of 100 x 100 x 90 m. The equivalent hydraulic conductivity for each block was obtained by flow calculations using stochastically generated fracture networks. The histograms of the calculated components for the hydraulic conductivity tensor are given in Figure 4-4. The shape of the distributions is approximately symmetric with a range of variability of about one order of magnitude.

With the help of this cellular upscaling method, it was possible to characterise the spatial variability for the equivalent hydraulic conductivity at the hectometric scale for the repository domain. This continuum type of description is applicable for modelling density effects at local scale.

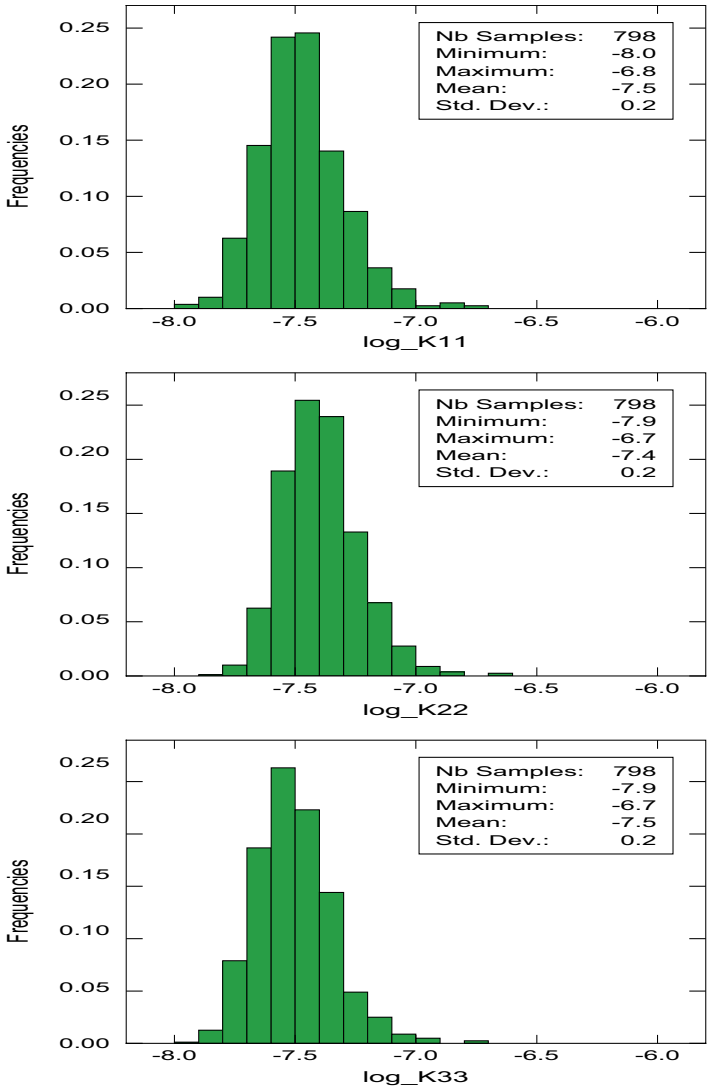

Figure 4-4. *Histograms of diagonal components for the equivalent hydraulic conductivity for the repository domain at local scale.*

4.2 Stochastic simulation at local scale

The hydraulic conductivity of the rock mass was simulated in 3 dimensions using the turning bands method /Chilès and Delfiner, 1999; Lantuéjoul, 2002/ implemented in NAMMU /Marsic et al, 2001/. The result was a Gaussian normalised simulation of the log-hydraulic conductivity spatially correlated (with a correlation length of 150 m) with values generated for every element of the mesh (see Table 4-2). This simulation was scaled according to the parameters related to the depth zonation defined in Table 3-1.

Table 4-2. Stochastic realisation: hydraulic conductivity statistics for the rock mass of the local model.

Depth (m)	Geometric mean of hydraulic conductivity (m/s)	Standard deviation (log 10)	Number of elements
0–35	$1.7 \cdot 10^{-7}$	0.46	14,400
	$(3.2 \cdot 10^{-7})$*		
35–875	$1.3 \cdot 10^{-8}$		
	$(4.6 \cdot 10^{-8})$*	0.36	289,200
875–1500	$5.2 \cdot 10^{-9}$		
	$(1.0 \cdot 10^{-8})$*	0.32	187,200

* Geometric mean including fracture zones

The fracture zones were defined implicitly as deterministic features using the IFZ method (Implicit Fracture Zone method implemented in NAMMU; /Marsic et al, 2001/). The fracture zones were integrated into the "stochastic" rock mass to obtain equivalent hydraulic properties; i.e. an equivalent (anisotropic) hydraulic conductivity and an equivalent porosity were calculated for each element in order to account for the hydraulic effects of a fracture zone intercepting it.

The results for the stochastic simulation of the hydraulic conductivity at local scale for the repository Variants I and II are displayed in Figure 4-5 and Figure 4-6. The longitudinal zones with high hydraulic conductivity values correspond to the fracture zones. The hydraulic conductivity for the repository (slab for Variant I or tunnels for Variant II) matches the value selected for the backfill material.

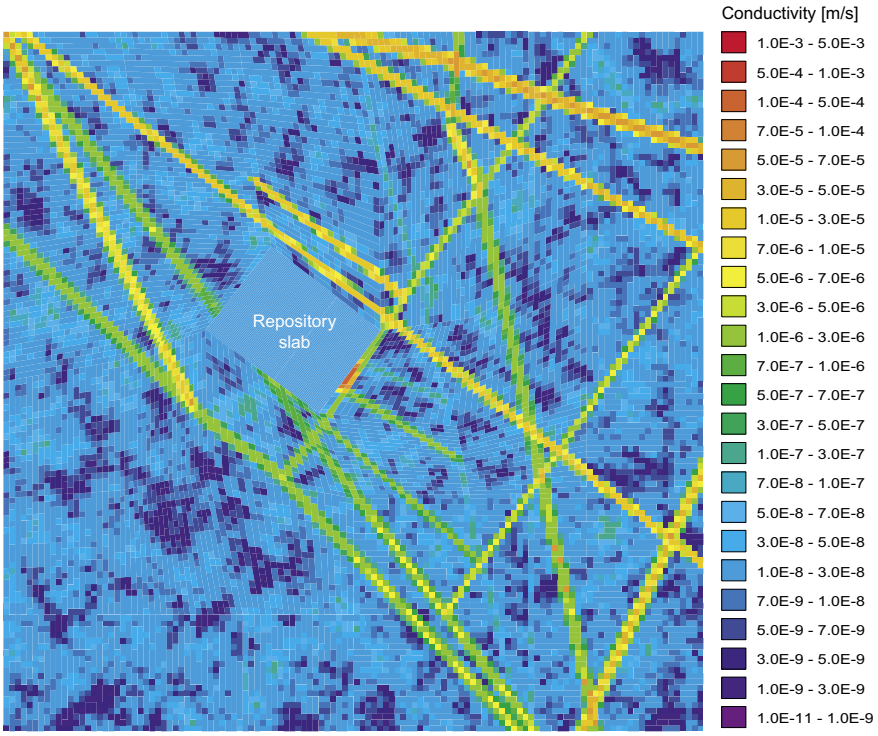

Figure 4-5. *Hydraulic conductivity field (Z-component) with implicit fracture zones for Variant I (repository slab within repository domain with uniform conductivity): horizontal cut at repository level.*

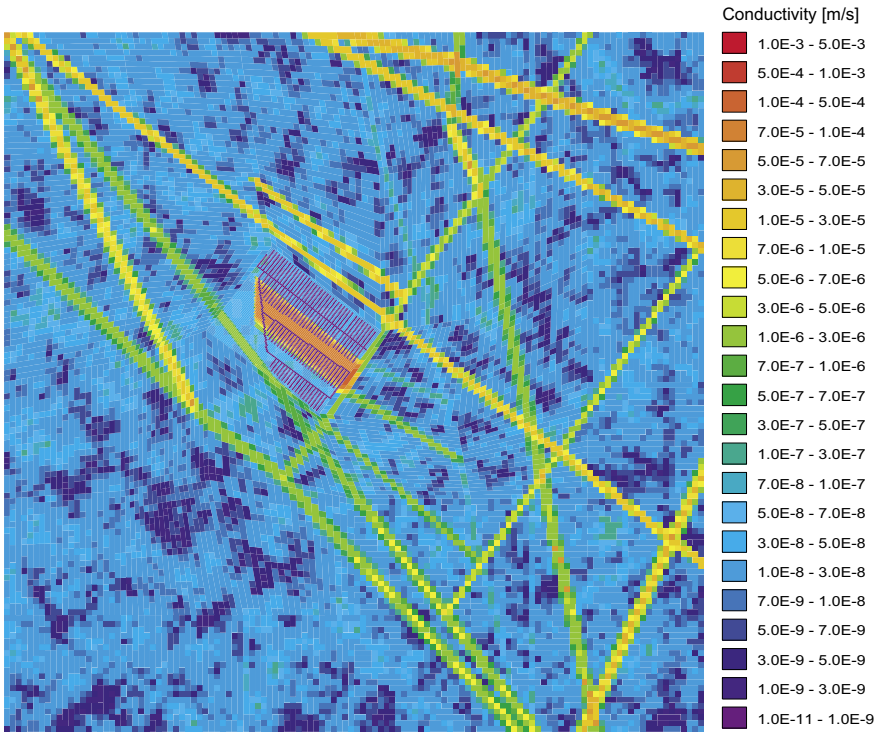

Figure 4-6. *Hydraulic conductivity field (Z-component) with implicit fracture zones for Variant II (repository with tunnels within repository domain with variable conductivity): horizontal cut at repository level.*

4.3 Modelling repository impact

Salt simulations at local scale were performed using the "stochastic" hydraulic conductivity for the rock mass, the implicit fractures zones and the equivalent hydraulic conductivity upscaled from the repository scale. In order to analyse the effects of density-driven flow in the phases of operation and post-closure of the repository, transient-mode calculations were run for a total duration of 300 a.

4.3.1 Initial conditions

Initial salt conditions

From the surface down to a depth of 500 m, the initial salinity (defined in % by weight) was specified to be zero. Starting at a depth of 500 m, a linear increase was prescribed to a maximum of 10% salinity at the depth of 2,100 m. Therefore, at the base of the model (depth of 1,500 m), the salinity was equal to 6.25% (see Figure 4-7).

Initial flow conditions

The initial flow conditions were taken from a simulation performed under steady-state conditions with a fixed salt profile (corresponding to the initial salt conditions; see Figure 4-7) in the absence of the repository (see Figure 4-8 and Figure 4-9).

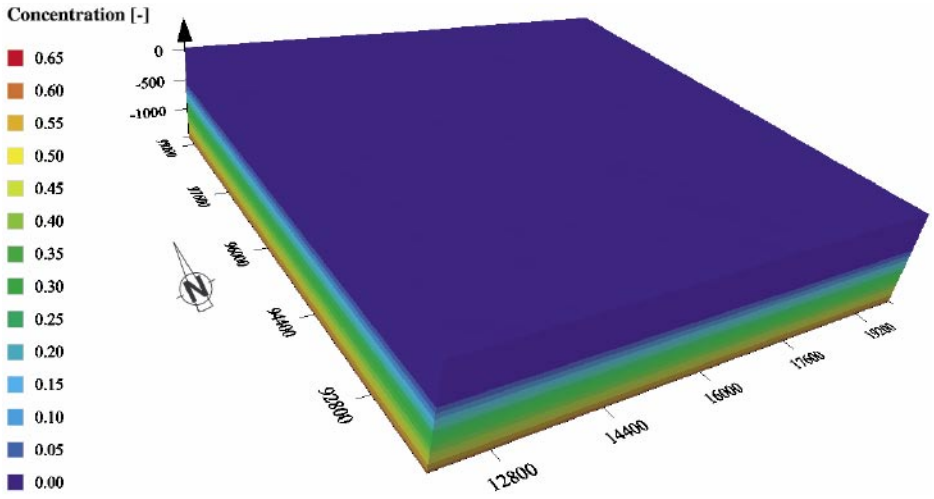

Figure 4-7. *Initial salt conditions (relative concentration).*

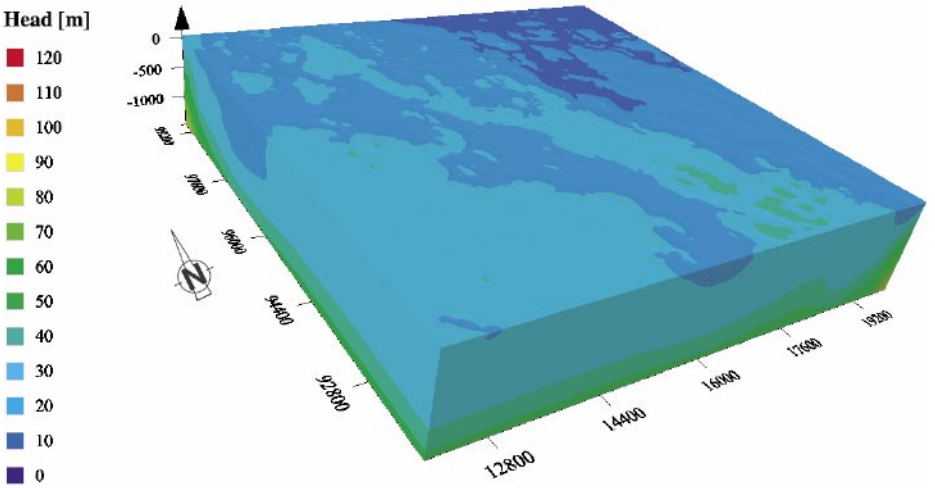

Figure 4-8. *Initial flow conditions: 3D block diagram (equivalent freshwater head).*

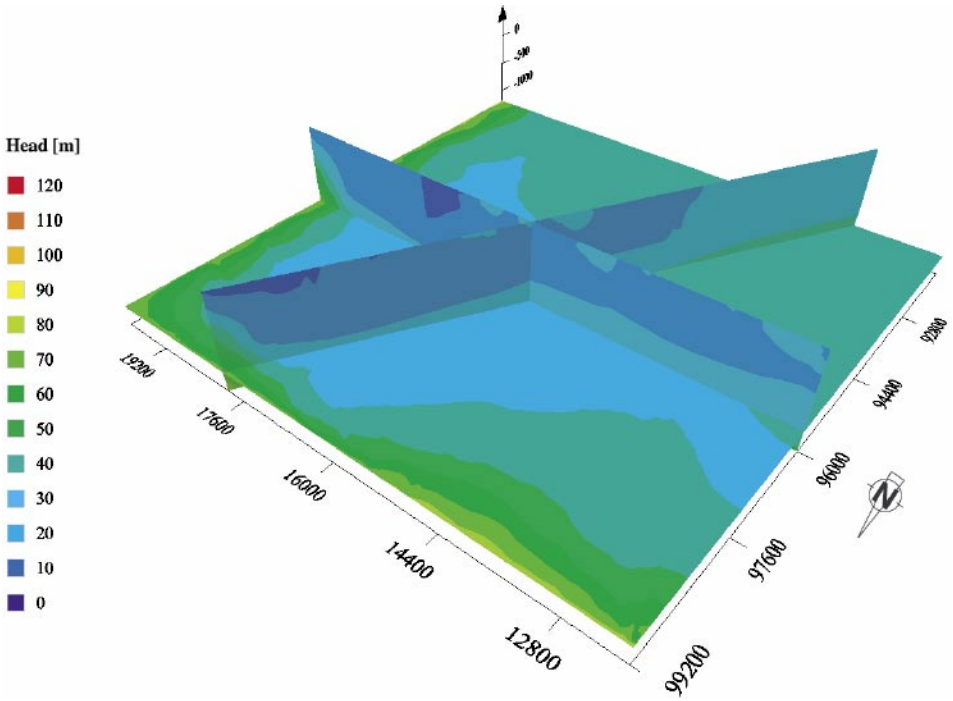

Figure 4-9. *Initial flow conditions: intersecting cuts (equivalent freshwater head).*

4.3.2 Boundary conditions

The boundary conditions for flow were the following:

- Along the top surface of the model: a fixed potential according to the topography.
- On the sides of the model: hydrostatic boundary conditions imposed as follows /Marsic et al, 2002/;

$$\frac{\partial p^R(x,t)}{\partial z} + \mathbf{g}(\rho(x,t) - \rho_0) = 0, \quad \text{with } q_z = 0$$

- For the base of the model: no-flow boundary conditions.
- In the repository/tunnels: atmospheric pressure at all nodes for the phase of repository operation (100 a).

The boundary conditions for transport were as follows:

- On the top surface of the model: the concentration of salt for the infiltrating water was set to zero.
- On the sides of the model, the following relative concentration was imposed:
  - from 0 to 500 m depth: zero concentration and
  - from 500 to 1,500 m depth: a linear increase of the concentration, reaching the value of 0.625 at 1,500 m.
- For the base boundary, no diffuse flux was prescribed.

- In the repository/tunnels: for the phase of repository operation, hole(s) were introduced in the finite-element mesh at the location(s) of the repository/tunnels. No diffuse flux was assigned to the walls of the hole(s).

4.3.3 Salt-water simulations

The salt-water simulations performed at local scale consist of three phases: (1) an initial steady-state phase, (2) a transient desaturation phase corresponding to the duration of repository operation (100 a) and (3) a transient resaturation phase related to the period of repository post-closure (200 a). The values for the hydraulic conductivity of the repository were assigned according to the phases (see Tables 4-3 to 4-6). Simulations at local scale were first carried out in 2 dimensions to gain understanding of the system response and then in 3 dimensions including all the available data for the two variants (cf Figure 4-1).

Table 4-3. 2D Simulation L1: repository box.

Initial phase K_{box} (m/s)	Desaturation phase K_{box} (m/s)	Resaturation phase $K_{box\_backfill}$ (m/s)
$4 \cdot 10^{-8}$	hole	$1.0 \cdot 10^{-10}$

Table 4-4. 3D Simulation L2 (reference, Variant I): repository slab.

Initial phase		Desaturation phase		Resaturation phase	
K_{slab} (m/s)	$K_{repo-domain*}$ (m/s)	K_{slab} (m/s)	$K_{repo-domain*}$ (m/s)	$K_{slab\_backfill}$ (m/s)	$K_{repo-domain*}$ (m/s)
$4 \cdot 10^{-8}$	$4 \cdot 10^{-8}$	hole	$4 \cdot 10^{-8}$	$1.0 \cdot 10^{-10}$	$4 \cdot 10^{-8}$

*repo_domain refers to the domain surrounding the repository slab

Table 4-5. 3D Simulation L3 (backfill sensitivity for Variant I): repository slab.

Initial phase		Desaturation phase		Resaturation phase	
K_{slab} (m/s)	$K_{repo-domain*}$ (m/s)	K_{slab} (m/s)	$K_{repo-domain*}$ (m/s)	$K_{slab\_backfill}$ (m/s)	$K_{repo-domain*}$ (m/s)
$4 \cdot 10^{-8}$	$4 \cdot 10^{-8}$	hole	$4 \cdot 10^{-8}$	**$1.0 \cdot 10^{-8}$**	$4 \cdot 10^{-8}$

Table 4-6. 3D Simulation L4 (Variant II): repository with tunnels.

Initial phase		Desaturation phase		Resaturation phase	
K_{tunnel} (m/s)	$K_{repo-domain*}$ (m/s)	K_{tunnel} (m/s)	$K_{repo-domain*}$ (m/s)	$K_{tunnel\_backfill}$ (m/s)	$K_{repo-domain*}$ (m/s)
$K_{DFN}(x)$*	**$K_{DFN}(x)$***	hole	**$K_{DFN}(x)$***	$1.0 \cdot 10^{-10}$	**$K_{DFN}(x)$***

*spatially variable hydraulic conductivity (cf Section 4.1)

4.3.4 2D salt-water simulations

The 2D model was orientated in an E-W direction and defined along an 8,000 x 1,500 m cut (cf Figure 3-1). This model orientation is advantageous with respect to the objective of gaining system understanding and an understanding of the chosen simplifications.

For the 2D salt-water simulations, the hydraulic conductivity for the rock mass was considered uniform according to the depth zonation provided in Table 3-1. The repository was regarded as a simple box with a length of 1,500 m, a height of 20 m and placed at a depth of 400 m. No repository domain was defined to surround the box. The remaining parameters and the initial and boundary conditions were identical to the 3D case (cf Sections 4.3.1 and 4.3.2).

After 100 a of desaturation the simulation results (see Figure 4-10) show the strong drainage effect caused by the atmospheric pressure conditions in the open repository. The steepest gradients are found above the repository, indicating that the majority of the water enters the repository through the top surface. However, the repository also drains water laterally and from the lower, salty parts of the model. The most notable impact of the repository on the salt distribution is a large up-coning effect; i.e. the initial salt profile (see Figure 4-7) is deformed and salt water is attracted upwards toward the repository (see Figure 4-11). The relative concentration of salt in the water entering the open repository after 100 a is between 0.1 and 0.15, corresponding to a salinity range of 1.0–1.5%.

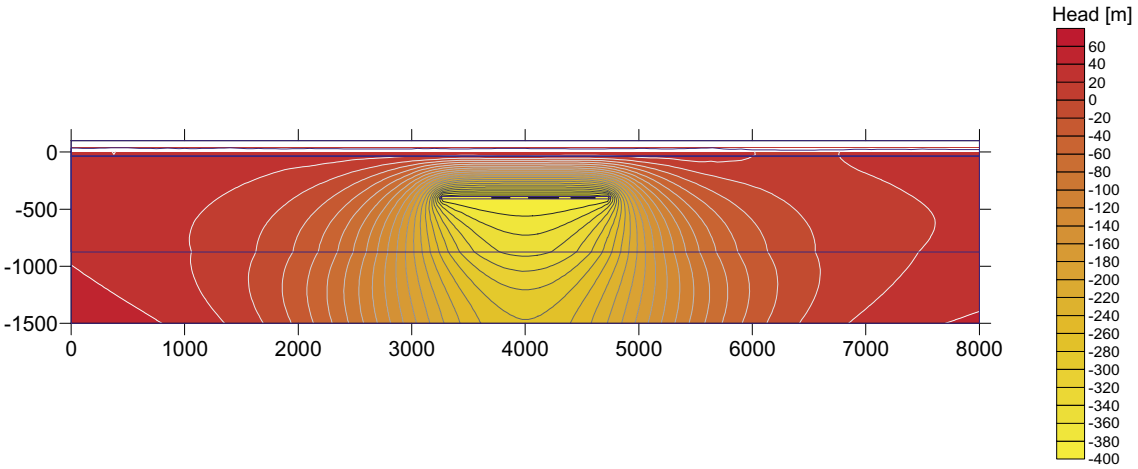

Figure 4-10. *Simulation L1: phase of desaturation at 100 a (equivalent freshwater head).*

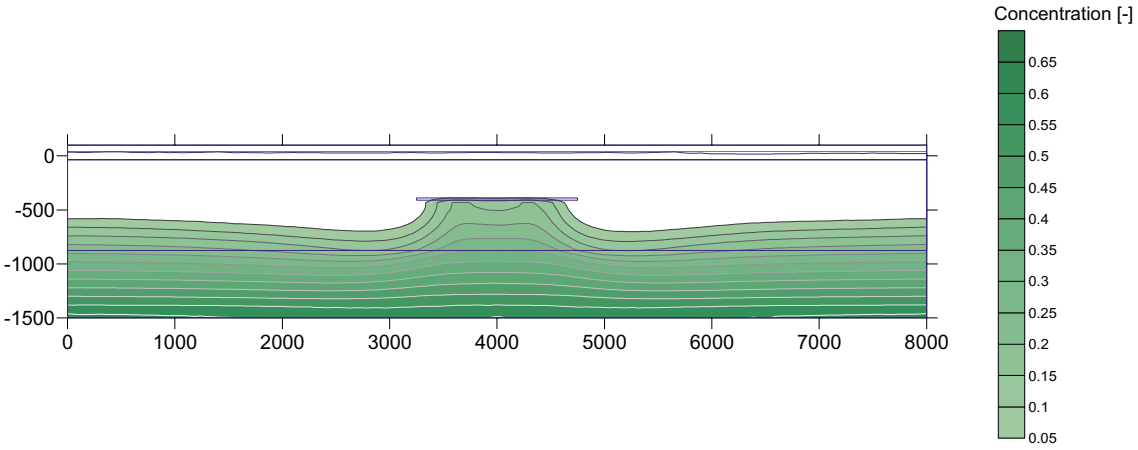

Figure 4-11. *Simulation L1: phase of desaturation at 100 a (relative concentration).*

After 100 a of repository operation under atmospheric conditions (i.e. the desaturation phase), the repository is closed and backfilled with material having a hydraulic conductivity of 10^{-10} m/s (cf Table 4-3). In other words, atmospheric conditions no longer prevail. The simulation of the post-closure resaturation phase was computed for a duration of 25 a. The resulting flow field reveals that the impact of repository operations appears no longer visible after 25 a (see Figure 4-12); evidence of the operation phase has vanished under the resaturation conditions. This result is confirmed by the simulated concentration distribution: the up-coning effect observed during repository operation has disappeared (see Figure 4-13).

Simulation L1_F was performed in order to analyse the effects of a fracture zone (with a hydraulic conductivity equal to 10^{-5} m/s) intersecting the repository. The results for the desaturation phase illustrate the role played by the fracture zone in distorting the flow field (see Figure 4-14) with the possibility of intensifying up-coning effects (see Figure 4-15).

For the resaturation phase, the results obtained for simulation L1_F were comparable to those for case L1 without fracture zone.

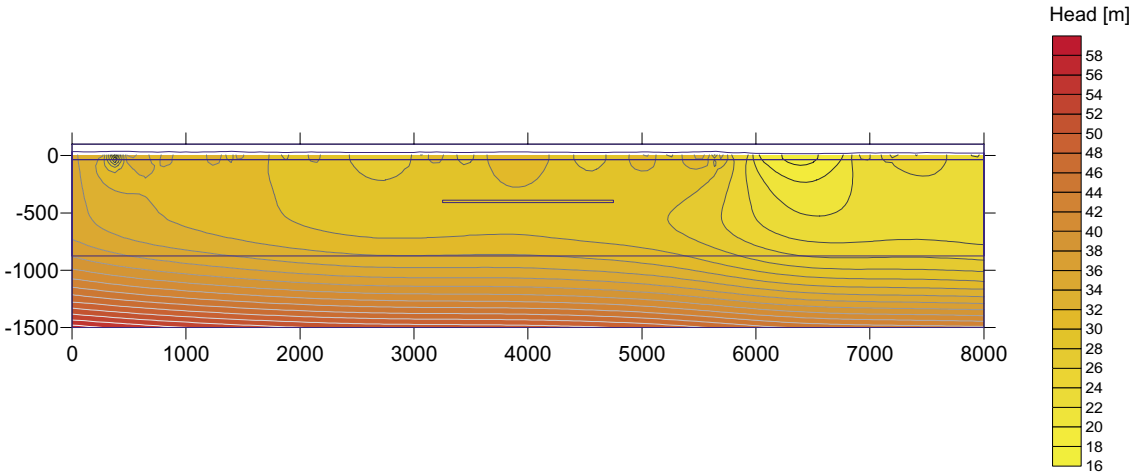

Figure 4-12. *Simulation L1: resaturation phase, 25 a after repository closure (equivalent freshwater head).*

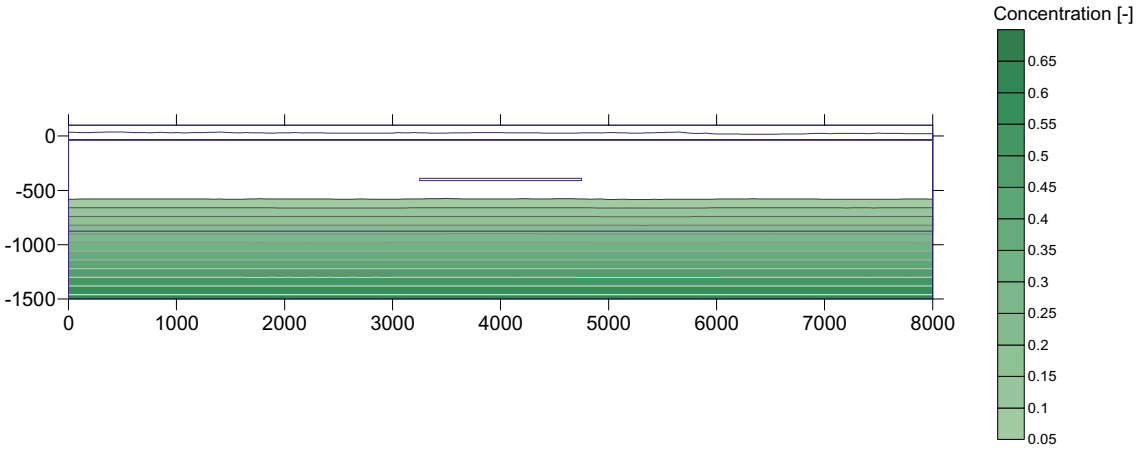

Figure 4-13. *Simulation L1: resaturation phase, 25 a after repository closure (relative concentration).*

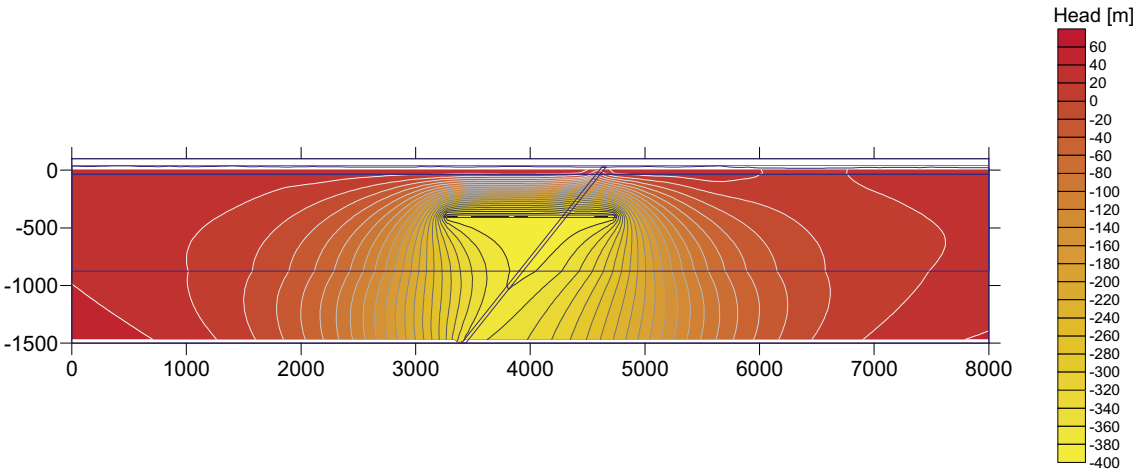

Figure 4-14. *Simulation L1_F: phase of desaturation at 100 a (equivalent freshwater head).*

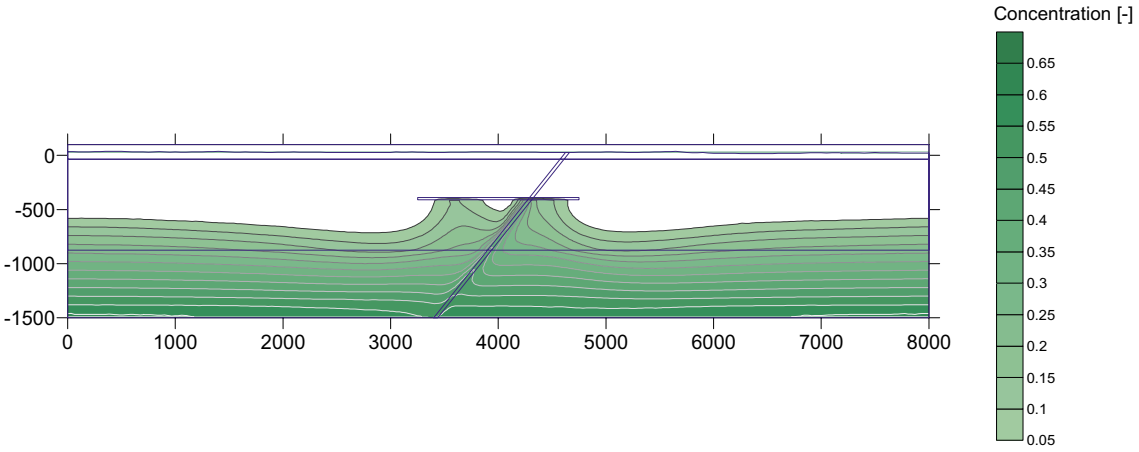

Figure 4-15. *Simulation L1_F: phase of desaturation at 100 a (relative concentration).*

4.3.5 3D salt-water simulations

The results of simulation L2 (reference case) after a 100 a desaturation phase show the strong impact of the repository on the flow field (see Figure 4-16 and Figure 4-17) and on the concentration in terms of up-coning (see Figure 4-18). Fracture zones play an important role in terms of carrying freshwater from the surface to greater depths.

The results of simulation L2 show that the impact of the repository seems to have vanished after the 200 a resaturation phase. In particular, perturbations in the flow field (see Figure 4-19) are no longer apparent and the concentration (see Figure 4-20) is affected predominantly by fractures.

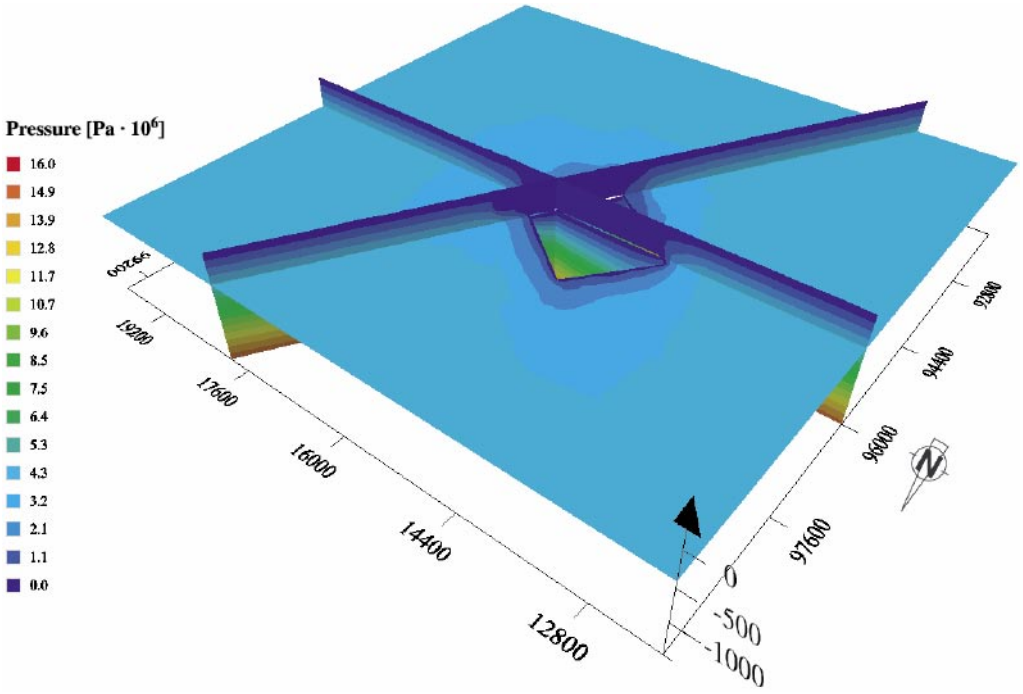

Figure 4-16. *Simulation L2 (pressure): after 100 a of desaturation; horizontal cut at repository level.*

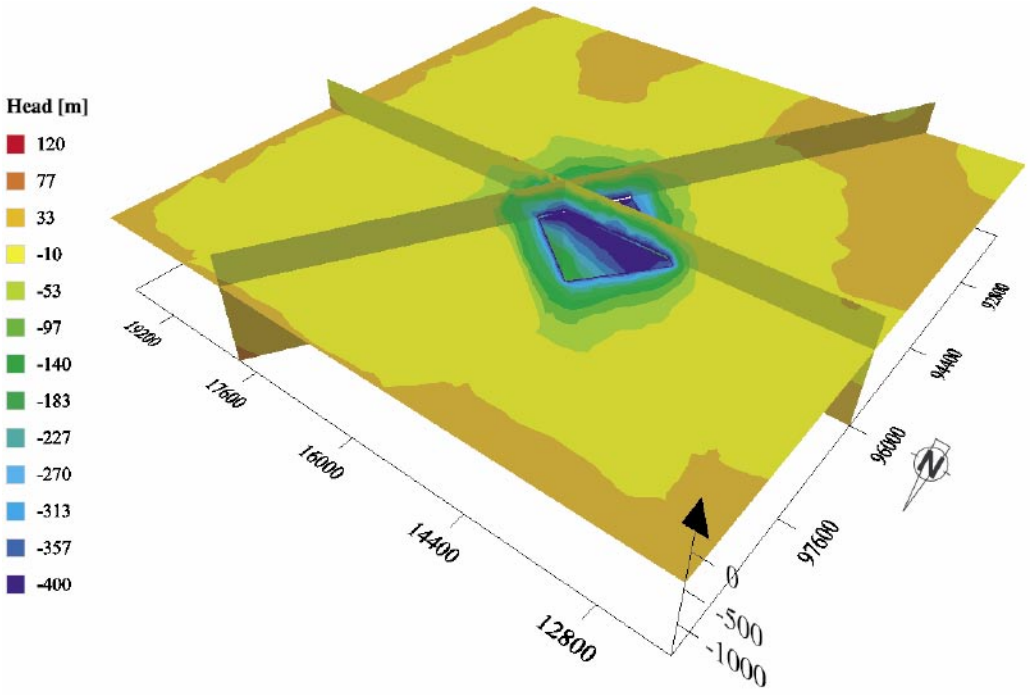

Figure 4-17. *Simulation L2 (equivalent freshwater head): after 100 a of desaturation; horizontal cut at repository level.*

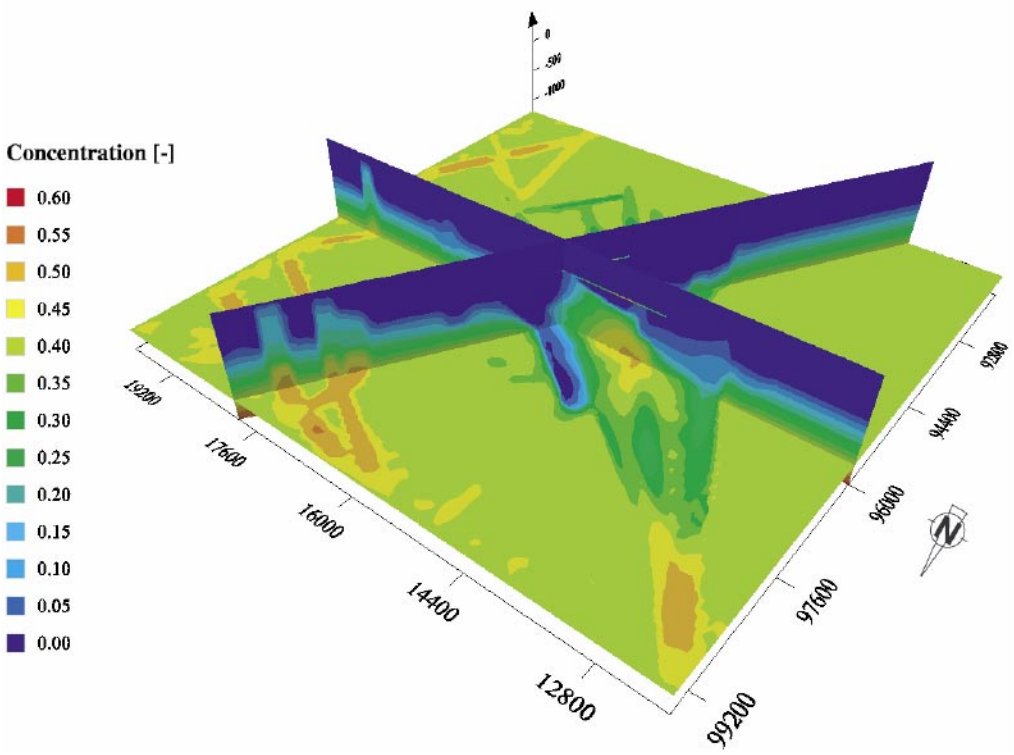

Figure 4-18. *Simulation L2 (relative concentration): after 100 a of desaturation; location of the repository indicated by a horizontal line in the cuts.*

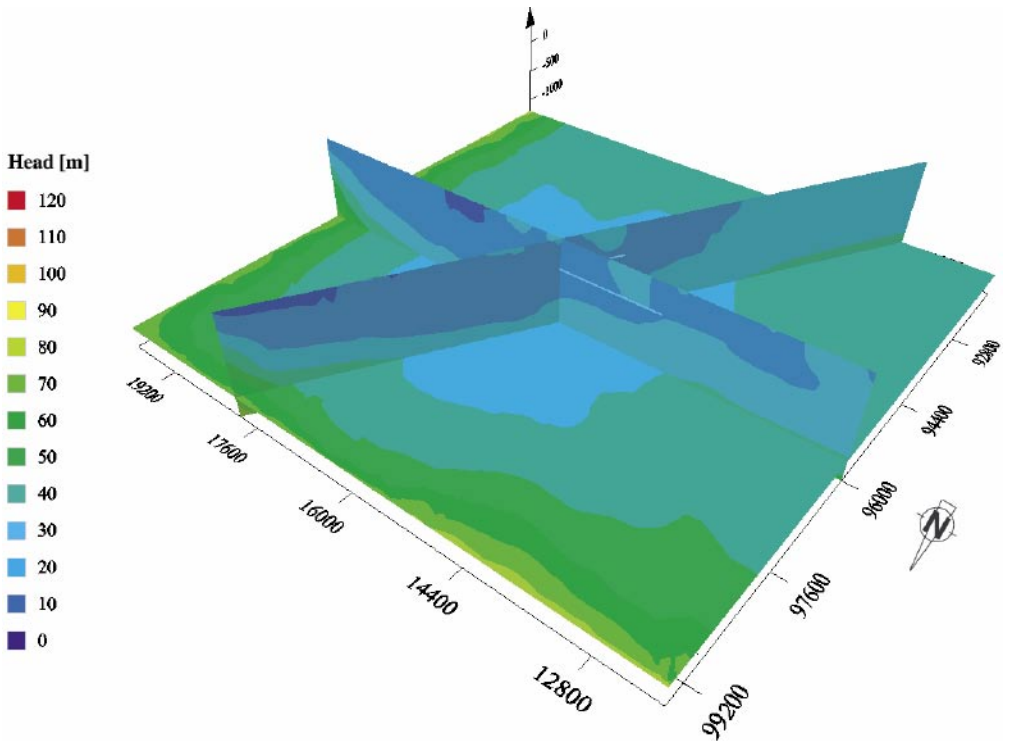

Figure 4-19. *Simulation L2 (equivalent freshwater head): resaturation phase, 200 a after repository closure; location of the repository indicated by a horizontal line in the cuts.*

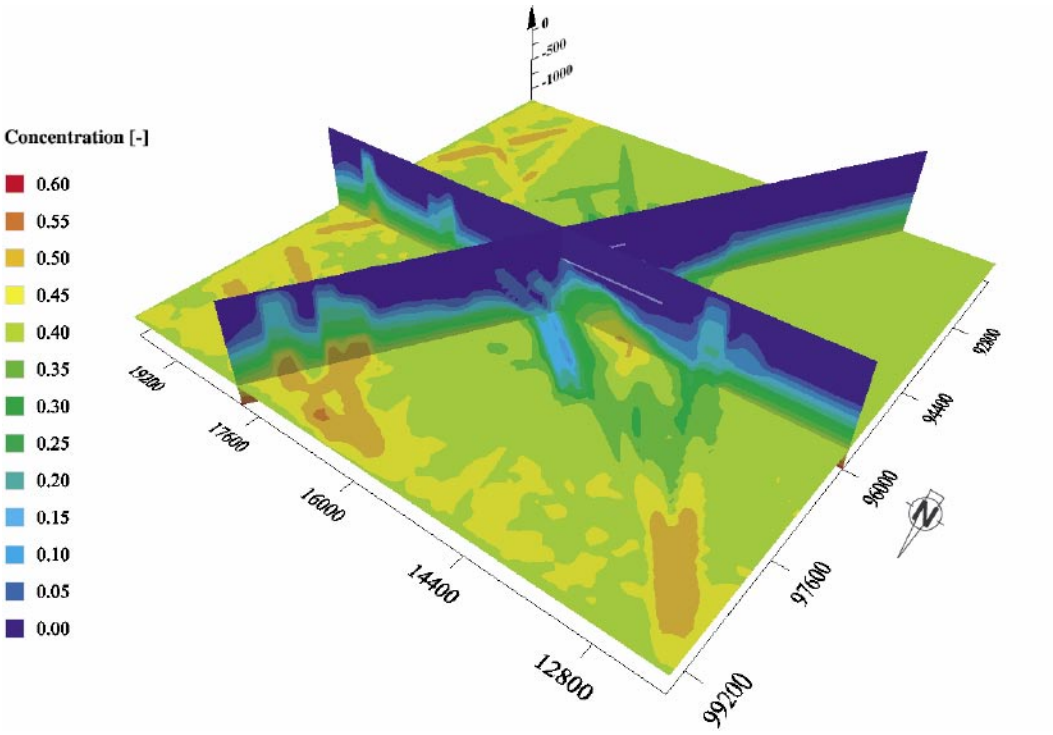

Figure 4-20. *Simulation L2 (relative concentration): resaturation phase, 200 a after repository closure; location of the repository indicated by a horizontal line in the cuts.*

For the resaturation phase of simulation L3, the hydraulic conductivity of the backfill was increased by a factor of 100. The desaturation phases of L2 and L3 are identical because they share the same parameters (cf Tables 4-4 and 4-5). After 200 a of resaturation, the results of simulation L3 are very similar to those from simulation L2 in terms of the flow (see Figure 4-21) and concentration fields (see Figure 4-22). The more permeable backfill in the repository seems to have almost no influence at local scale.

Simulation L4 is a variant of simulation L2 where the tunnels of the repository are explicitly considered (cf Section 4). For the desaturation phase at 100 a, due to the smaller repository volume considered, the results (see Figure 4-23) show a slightly reduced impact of the repository on the flow field compared to simulation L2 (cf Figure 4-17). This outcome also explains why the extent of the up-coning effect (see Figure 4-24) is decreased in comparison to the results of simulation L2 (cf Figure 4-18). For the phase of desaturation (at 200 a), the obtained results for simulation L3 (see Figure 4-25) are similar in terms of flow and concentration fields to simulation L2 (cf Figure 4-20).

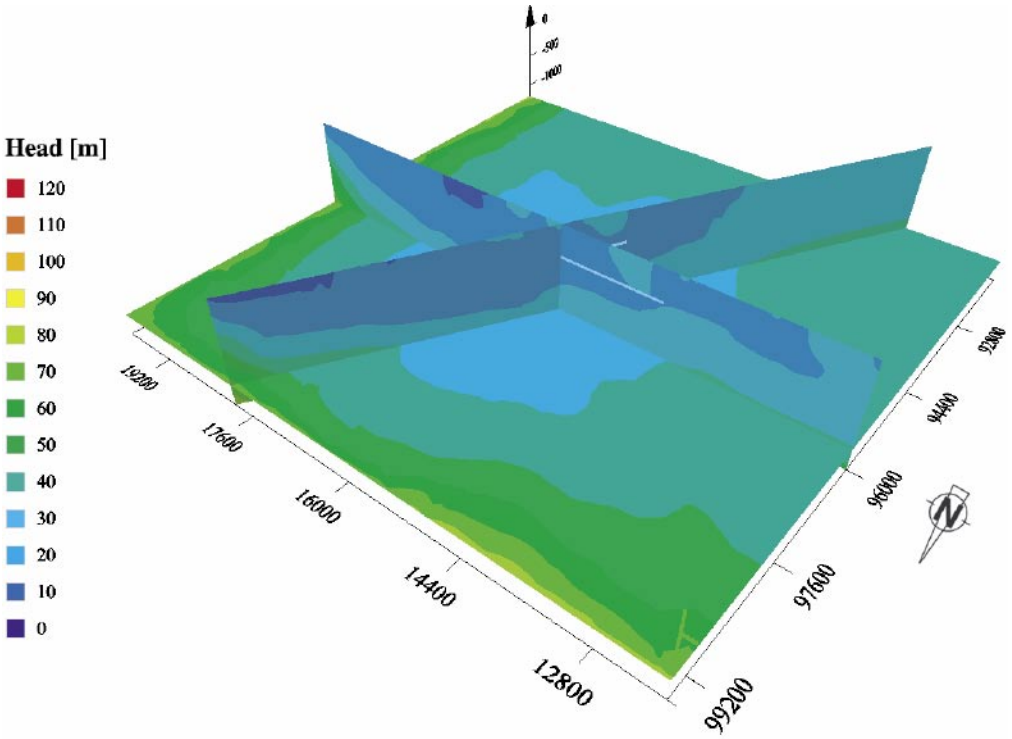

Figure 4-21. *Simulation L3 (equivalent freshwater head): resaturation phase, 200 a after repository closure; location of the repository indicated by a horizontal line in the cuts.*

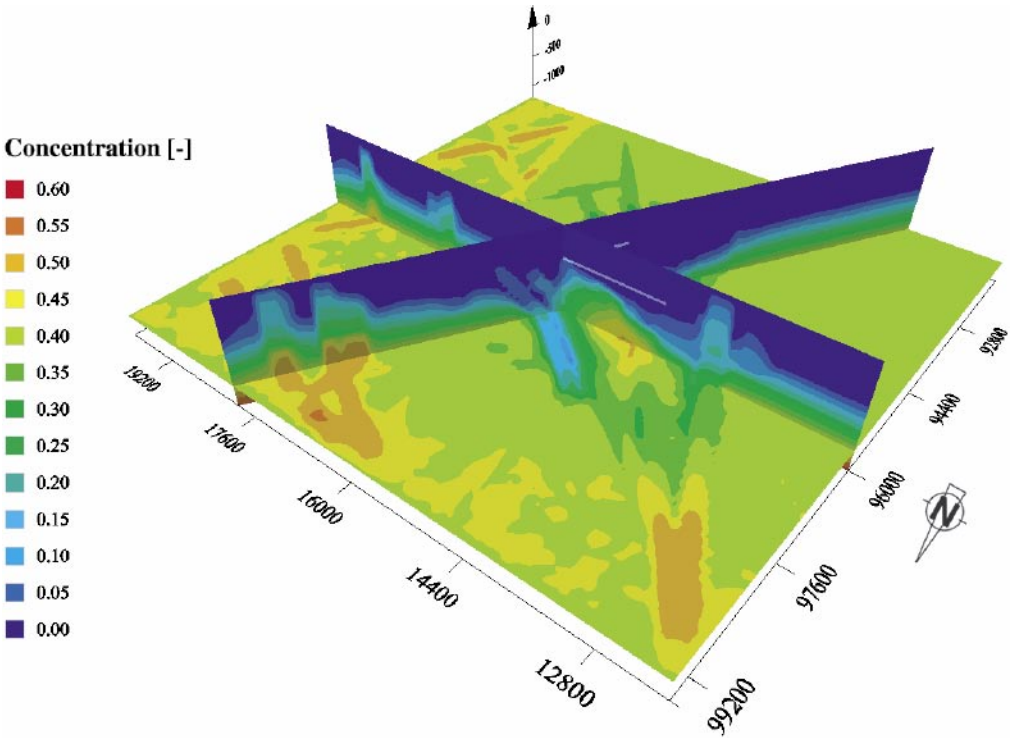

Figure 4-22. *Simulation L3 (relative concentration): resaturation phase, 200 a after repository closure; location of the repository indicated by a horizontal line in the cuts.*

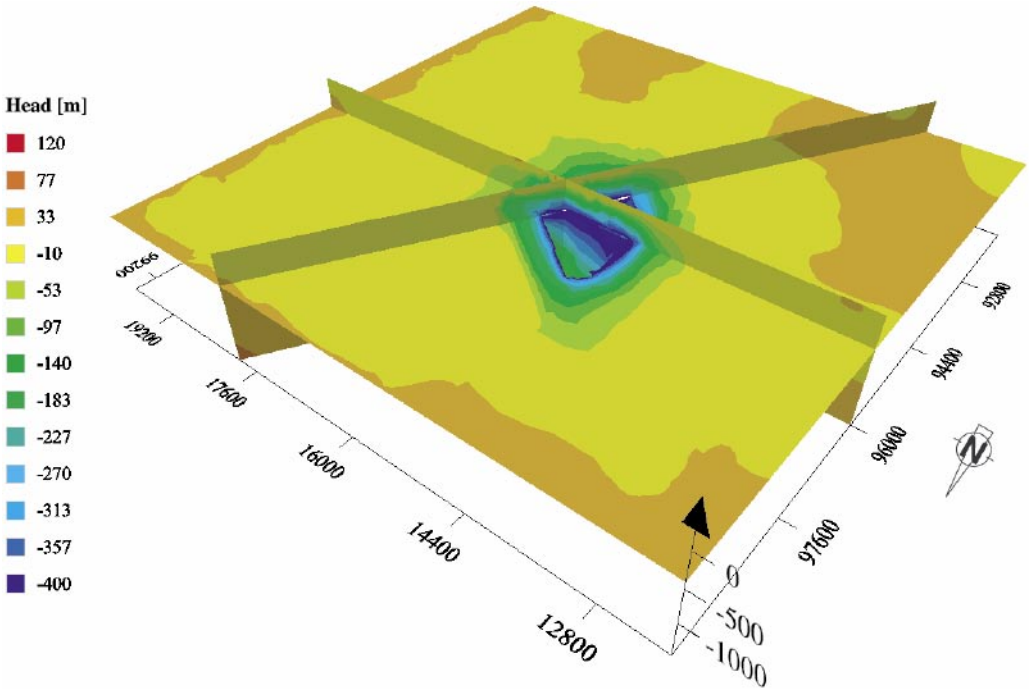

Figure 4-23. *Simulation L4 (equivalent freshwater head): phase of desaturation at 100 a; horizontal cut at repository level.*

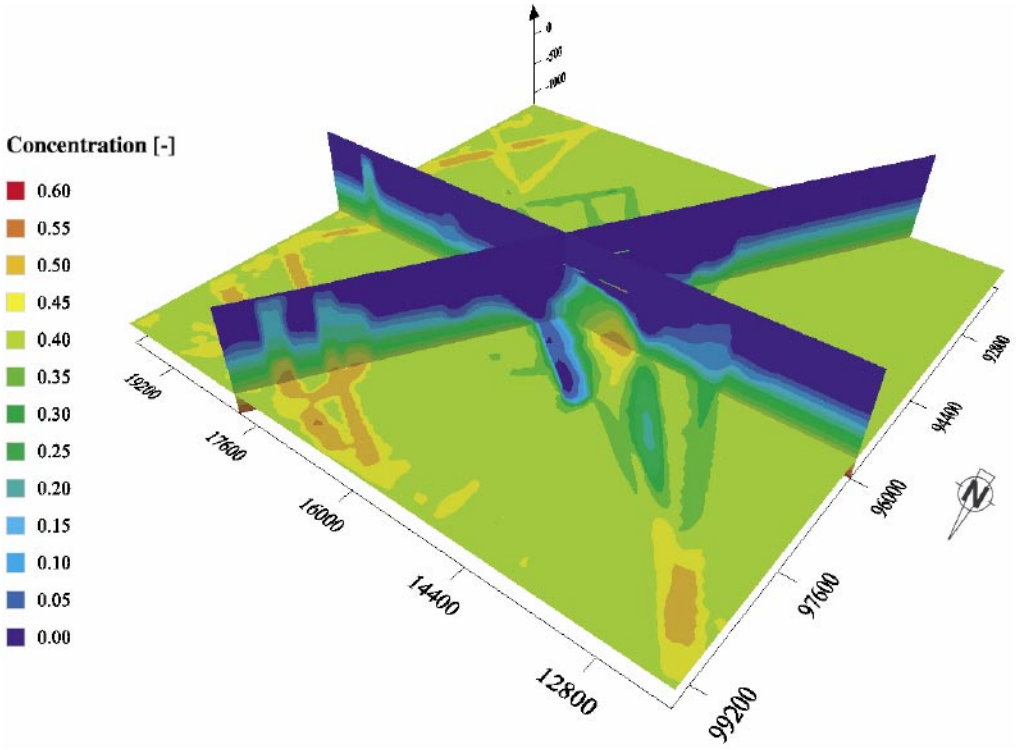

Figure 4-24. *Simulation L4 (relative concentration): phase of desaturation at 100 a; location of the repository indicated by a horizontal line in the cuts.*

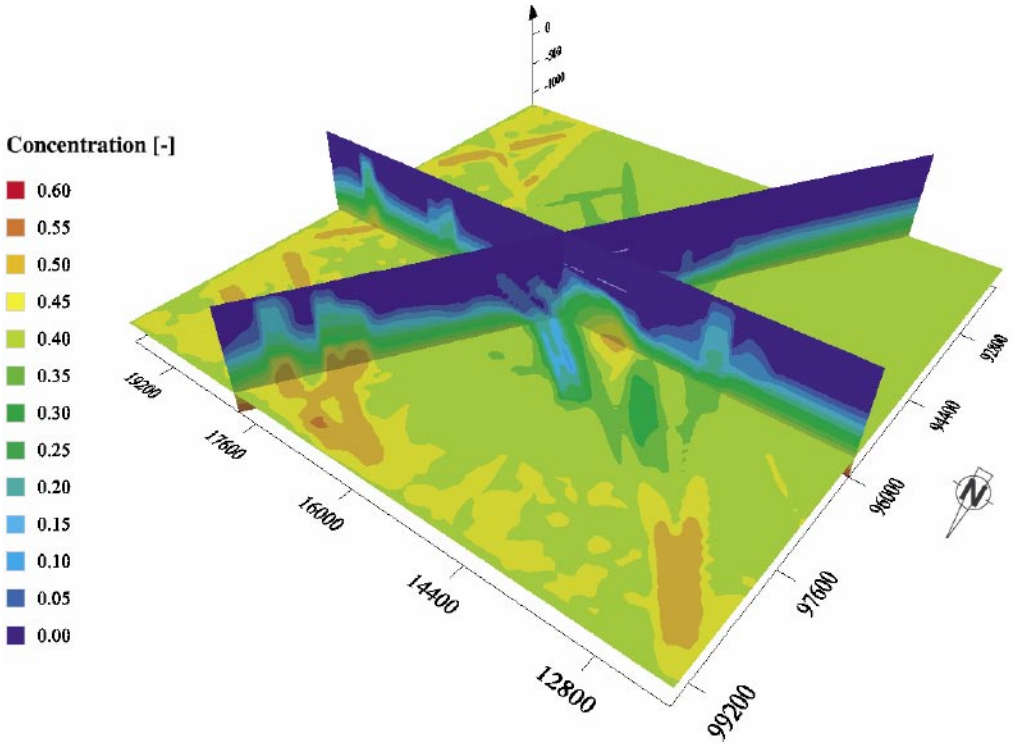

Figure 4-25. *Simulation L4 (relative concentration): phase of resaturation at 200 a; location of the repository indicated by a horizontal line in the cuts.*

4.3.6 Performance measures

Three performance measures were considered for the evaluation of the repository impact:

- Resaturation time.
- Maximum salt concentration at repository level.
- Total inflow to the repository during resaturation phase.

The resaturation time, starting at repository closure, corresponds to the time at which the effects of the operation phase are no longer perceptible in the flow field. The resaturation time was evaluated by calculating the maximum head differences observed at every node of the model between two time steps.

After 20 years of resaturation, the maximum head difference observed between two time steps reaches an approximately constant value for simulation L2 (see Table 4-7); i.e. after a period of about 20 a, the impact of the phase of repository operation has disappeared. The minor residual differences observed are related to transient density effects.

Increasing the hydraulic conductivity of the backfill (simulation L3) causes similar results. It has no effect on the resaturation time. An explicit description of the tunnels for the repository leads to a reduction of the resaturation time (corresponding to a period of ca 15 a). This reduction is caused by the diminution in volume of the repository which decreases the impact of the repository on the flow field.

Table 4-7. Evaluation of resaturation time.

Time step (a)	Simulation L2 Equivalent freshwater head (maximum difference in m)	Simulation L3 Equivalent freshwater head (maximum difference in m)	Simulation L4 Equivalent freshwater head (maximum difference in m)
5–10	27.48	27.49	6.95
10–15	2.10	2.09	0.49
15–20	0.45	0.45	0.44
20–30	0.77	0.77	0.72
30–40	0.66	0.66	0.65
40–50	0.61	0.61	0.63

The maximum (relative) concentration at repository level (depth of 420 m) was evaluated for the phases of repository operation and post-closure. The results are presented in Table 4-8 for simulations L2 and L3 and L4. Between the phases of desaturation and resaturation, the decrease in the maximum observed concentration is respectively 33% and 44% for simulation L2 and L4. With the closing of the repository, the up-coning effect gradually disappears and the concentration is then related to the unperturbed density-driven flow field.

For simulation L3, slightly smaller results in terms of maximum concentration were obtained. Due to the increased hydraulic conductivity, the barrier effect of the repository is weakened so that more freshwater flows to greater depth and potentially reduces the observed concentration.

For simulation L4, the decrease in maximum concentration in comparison to simulation L2 are related to the lesser impact of the explicit repository on the flow field.

Table 4-8. Evaluation of maximum (relative) concentration at repository level for desaturation and resaturation phases.

Time (a)	Simulation L2 Concentration maximum (–)	Concentration relative to model maximum (%)	Simulation L3 Concentration maximum (–)	Concentration relative to model maximum (%)	Simulation L4 Concentration maximum (–)	Concentration relative to model maximum (%)
50	0.169	27	*	*	0.149	24
100	0.151	24	*	*	0.119	19
150	0.114	18	0.105	17	0.084	13
300	0.099	16	0.089	14	0.090	14

* For the desaturation phase, simulation L3 is identical to simulation L2.

The bold line indicates repository closure at 100 a

The inflow to the repository was calculated by integrating the flux through each of the faces of the repository slab during repository operation. The results show that the calculated inflow to the repository is steady already after a few years (see Table 4-9). This is explained by the relatively large diffusivity (ca 10^{-2} m^2/s) occurring at the repository level. Due to the fixed head imposed as boundary conditions at the top surface of the model, the calculated values represent upper bounds for the inflow to the repository (see Appendix).

Table 4-9. Evaluation of total inflow to the repository in the desaturation phase.

Time cumulated (a)	Simulation L2 Total inflow (m^3/s)	Simulation L4 Total inflow (m^3/s)
0.5	–4.671	–4.429
5	–4.651	–4.422
50	–4.651	–4.421
100	–4.650	–4.421

For the desaturation phase, simulation L3 is identical to simulation L2

4.4 Environmental impact issue

The repository is situated at a depth of 400 m and provides for atmospheric conditions during the operation phase. These strong drawdown conditions induced by the open repository are likely to cause near-surface effects (e.g. dry wells) which need to be analysed and quantified with respect to their impact in space and time using numerical calculations. One critical issue is the selection of an adequate boundary condition for the top surface of the model. Some scoping freshwater calculations were performed in two dimensions in order to compare various types of boundary conditions (see Appendix). These calculations have shown that the selection of a fixed head as boundary conditions along the model top surface is not adequate for near-surface assessment. Such evaluation would require the application of free surface boundary conditions for the numerical modelling of repository impact.

5 Conclusions and perspectives

A hydrogeological model was developed for Beberg with the aim of evaluating the impact of a repository (for the operational and post-closure phases) while accounting for the effects of density-driven flow. Two embedded scales were taken into account for this modelling study: a local scale at which the granitic medium was considered as a continuum and a repository scale, where the medium is fractured and therefore was regarded to be discrete.

The following step-wise approach was established to model density-driven flow at both repository and local scale: (a) modelling fracture networks at the repository scale, (b) upscaling the hydraulic properties to a continuum at local scale and (c) modelling density-driven flow to evaluate repository impact at local scale.

The results demonstrate the strong impact of the repository on the flow field during the phase of operation. The distribution of the salt concentration is affected by a large up-coning effect with increased relative concentration and by the presence of fracture zones carrying freshwater from the surface. The concentrations obtained for the reference case, expressed in terms of percentage with respect to the maximum (prescribed) value in the model, are as follows:

- ca 30% for the phase of desaturation, and
- ca 20% for the resaturation phase.

For the reference case, the impact of repository operations appears no longer visible after a resaturation period of about 20 a after repository closure; under resaturation conditions, evidence of the operational phase has already disappeared in terms of the observed hydraulic and concentration fields.

Sensitivity calculations have proven the importance of explicitly discretising repository tunnels when assessing resaturation time and maximum concentration values. Furthermore, the definition of a fixed potential as boundary condition along the model's top surface is likely to provide underestimated values for the maximum concentration and overestimated flow rates in the repository during the operational phase. Scoping calculations have shown that the results could be improved by applying free-surface boundary conditions when modelling the impact of the repository.

Modelling density-driven flow at local scale with a repository under atmospheric pressure conditions is feasible using CONNECTFLOW / NAMMU. Such non-linear problems are intrinsically difficult to solve and linked with numerical difficulties. In particular, we could overcome the numerous convergence issues but it was demanding in terms of computing performance. Concerning pre-processing, this study has allowed us to improve the integration of CONNECTFLOW / NAMMU within Colenco's computing environment. It is especially noteworthy that numerical calculations with complex geometries (e.g. repository layout with tunnels) have become possible.

During the phases of repository operation and post-closure, near-surface effects are likely to occur. The evaluation of their environmental impacts needs to be performed using a numerical model with specific boundary conditions (free surface type).

The following recommendations are proposed regarding additional work and open issues:

- Assessment of the environmental impacts in relation to the phases of repository operation and post-closure.
- Evaluation of repository impact using a more detailed geometry for the repository layout, such as introducing the shafts and access tunnels as well as including skin effect around the tunnels.
- Determination of repository impact by modelling density-driven flow including the rock matrix diffusion of salt.

The approach for modelling repository impact at Beberg has successfully described the assumed conditions and relevant processes. It may certainly serve as a well founded base for future modelling tasks to provide solutions to further questions.

6 References

Chilès J P, Delfiner P, 1999. Geostatistics: modelling spatial uncertainty, Wiley Series in Probability and Mathematical Statistics, 695p.

Cliffe K A, Morris S T, Porter J D, 1998. Assessment model validity document, NAMMU: a program for calculating groundwater flow and transport through porous media, SKB R-99-51, Svensk Kärnbränslehantering AB.

Dershowitz W, Eiben T, Follin S, Andersson A, 1999. SR 97- Alternative models project, discrete fracture network modelling for performance assessment of Aberg, SKB R-99-43, Svensk Kärnbränslehantering AB.

Gylling B, Marsic N, Hartley L, Holton D, 2003. Applications of hydrogeological modelling methodology using NAMMU and CONNECTFLOW – Task 1, 2, 3 and 4, SKB R-04-45, Svensk Kärnbränslehantering AB.

Gylling B, Walker D, Hartley L, 1999. Site-scale groundwater flow modelling of Beberg, SKB TR-99-18, Svensk Kärnbränslehantering AB.

Grinrod P, Herbert A, Roberts D, Robinson P, 1991. NAPSAC technical document, Stripa project, TR-91-31.

Hartley L, Boghammar A, Grundfelt B, 1998. Investigation of the large scale regional hydrogeological situation at Beberg using NAMMU, SKB TR-98-24, Svensk Kärnbränslehantering AB.

Lantuéjoul C, 2002. Geostatistical simulation: models and algorithms, Springer, 256p.

Marsic N, Hartley L, Sanchez-Friera P, Morvik A, 2002. Embedded regional/local –scale model of natural transients in saline groundwater flow illustrated using the Beberg site, SKB TR-02-22, Svensk Kärnbränslehantering AB.

Marsic N, Hartley L, Jackson P, Poole M, Morvik A, 2001. Development of hydrogeological modelling tools based on NAMMU, SKB TR-01-49, Svensk Kärnbränslehantering AB.

Marsic N, Gylling B, Grundfelt B, Hartley L, 2000. Modelling of the site scale hydrogeological situation at Beberg, SKB TR-00-14, Svensk Kärnbränslehantering AB.

Rhén I, Gustafson G, Stanfors R, Wikberg P, 1997. Äspö HRL – Geoscientific evaluation 1997/5. Models based on site characterisation 1986–1995. SKB TR-97-06, Svensk Kärnbränslehantering AB.

SR 97, 1999. Post-closure safety, SKB TR-99-06, Volume I. Svensk Kärnbränslehantering AB.

Svensson U, 1999. Subglacial groundwater flow at Äspö as governed by basal melting and ice tunnels, SKB R-99-38, Svensk Kärnbränslehantering AB.

Walker D, Rhén I, Gurban I, 1997. Summary of hydrogeologic conditions at Aberg, Beberb and Ceberg, SKB TR-97-23, Svensk Kärnbränslehantering AB.

Appendix

2D freshwater simulation

Geometry

The 2D model was orientated in an E-W direction and defined along an 8,000 x 1500 m cut (cf Figure 3-1). For the 2D freshwater simulations, the hydraulic conductivity for the rock mass was considered uniform according to the depth zonation specified in Table 3-1. The repository was regarded as a simple box with a length of 1,500 m and a height of 20 m, placed at a depth of 600 m /SR 97, 1999/. The depth was later modified by SKB to 400 m (cf Section 4.3.4). The influence of the repository depth should be negligible, since these 2D scoping calculations aim at comparing various types of surface boundary conditions.

Boundary and initial conditions

The boundary conditions for the 2D model were the following:

Along the top surface of the model:

- Option 1: fixed hydraulic potential given by the topography.
- Option 2: flow prescribed in terms of recharge (25 mm/a, after /Walker et al, 1997/).
- Option 3: free surface with recharge and exfiltration.

On the sides of the model:	hydrostatic boundary conditions prescribed with a fixed potential equal to the surface altitude of the respective side.
At the base of the model:	no-flow boundary conditions.
In the repository:	atmospheric pressure at all nodes for the phase of repository operation (100 a).

For the initial conditions without repository, steady-state calculations were performed for the three options of surface boundary conditions (see Figure A-1, Figure A-2 and Figure A-3). Fixed-head and free-surface conditions present similar and realistic results in terms of the flow field. Contrary to these, the initial conditions with recharge cause a potential field with values exceeding the topographic surface because there is no exfiltration possibility on the top surface. These unrealistic initial conditions were therefore abandoned for the transient calculations of option 2 and replaced by initial conditions with fixed head.

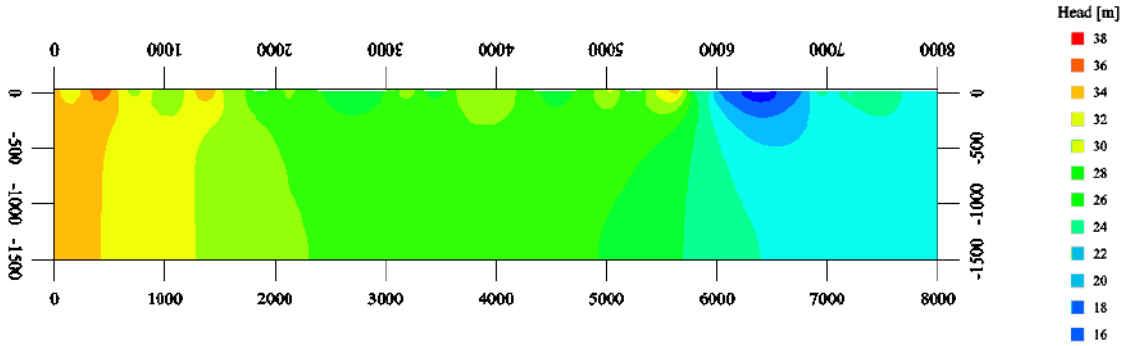

Figure A-1. *Initial conditions with fixed head (option 1).*

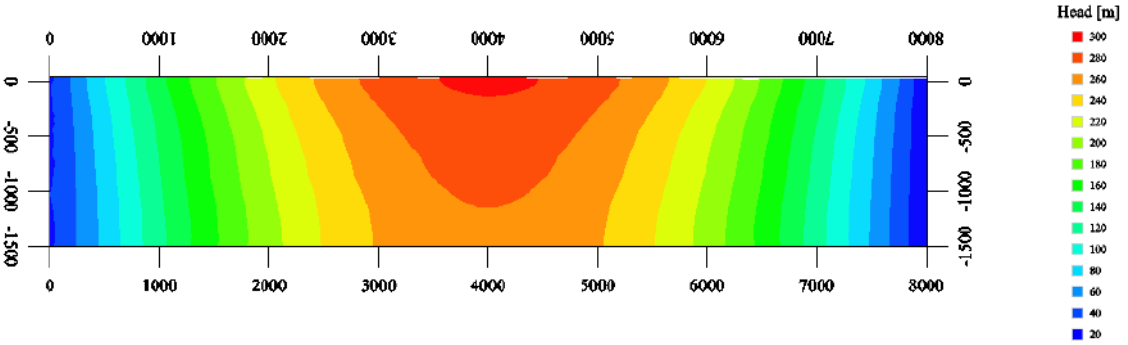

Figure A-2. *Initial conditions with recharge (option 2).*

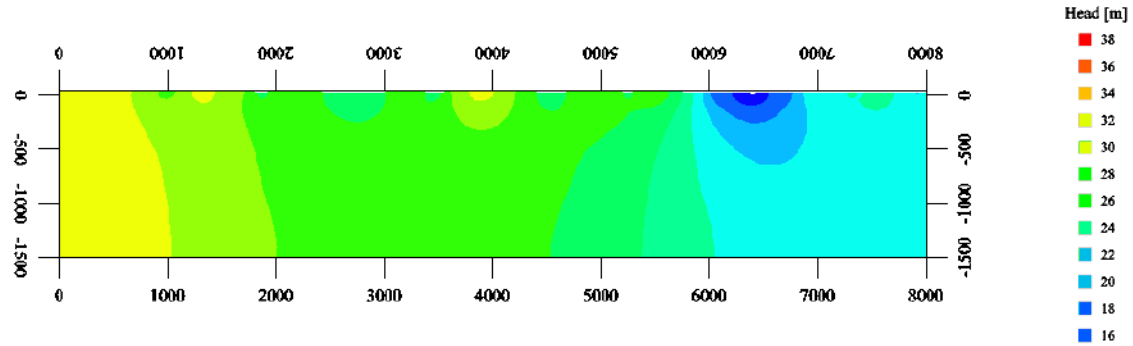

Figure A-3. *Initial conditions with free surface (option 3).*

Numerical aspects

The simulations were performed with the method of mixed hybrid finite elements using the code MYTHICS (**M**ixed **H**ybrid **T**ransfer **I**ntegrated **C**ode) developed at Colenco. This numerical method allows for the simultaneous calculation of hydraulic potential and flux in order to ensure a better approximation of the velocity field. In contrast to classical finite element methods, mass conservation is guaranteed at element level; i.e. the velocity field is continuous from one element to the next.

For free surface conditions the system of equations becomes non-linear. It is solved using an iterative method of Picard with a relaxation coefficient which is applied to the hydraulic potential to facilitate convergence. For each iteration, the solution of the linear flow system is achieved with the help of the iterative method of the preconditioned conjugate gradient applying the procedure of Eisenstat. An implicit scheme is used for time discretisation. The convergence criterion applied for the simulation with a free surface was about 1 m. For zones with negative pressure representing the unsaturated zones, the hydraulic conductivity is reduced by a factor of 10, allowing for a simplified description of flow under free surface conditions.

2D freshwater simulations

A 2D freshwater simulation consists of three phases (see Table A-1): (1) an initial steady-state phase, (2) a transient desaturation phase corresponding to the duration of repository operation (100 a) and (3) a transient resaturation phase related to the period of repository post-closure (200 a). Three simulations were performed corresponding to the options for the surface boundary conditions (see Table A-2).

Table A-1. Phases for freshwater simulations.

Initial phase K_{box} (m/s)	Desaturation phase K_{box} (m/s)	Resaturation phase $K_{box\_backfill}$(m/s)
$4 \cdot 10^{-8}$	Hole	$1.0 \cdot 10^{-10}$

Table A-2. Characteristics of freshwater simulations.

Simulation	Surface boundary conditions	Specifications	Recharge (mm/a)
L0_o1	Fixed head	Confined aquifer; no desaturation effects	Corresponding to ca 100–900
L0_o2	Prescribed flow	Confined aquifer; limited desaturation effects	25
L0_o3	Free surface + exfiltration	Unconfined aquifer; realistic desaturation effects	25

The results of the simulations with different boundary conditions (see Figure A-4, Figure A-5 and Figure A-6) show the strong drainage effect after 100 a of desaturation, due to the open repository under atmospheric pressure conditions. Simulation L0_o1 displays the steepest gradient above the repository in comparison to the other cases. This gradient results from the large differences in prescribed head values between the top surface and the repository. In terms of flow rate to the repository, simulation L0_o1 presents the largest value when compared to the other simulations (see Table A-3). For simulation L0_o3, the observed reduction in flow rate to the repository is related to a smaller recharge value (i.e. 25 mm/a) and to the decrease in hydraulic conductivity in the unsaturated zone (cf section on numerical aspects).

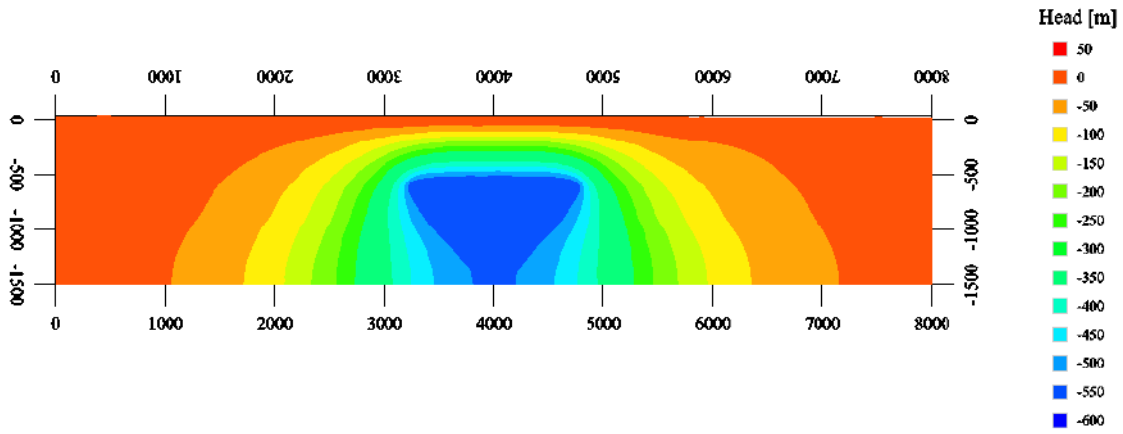

Figure A-4. *Simulation L0_o1 (hydraulic head): phase of desaturation at 100 a (fixed head).*

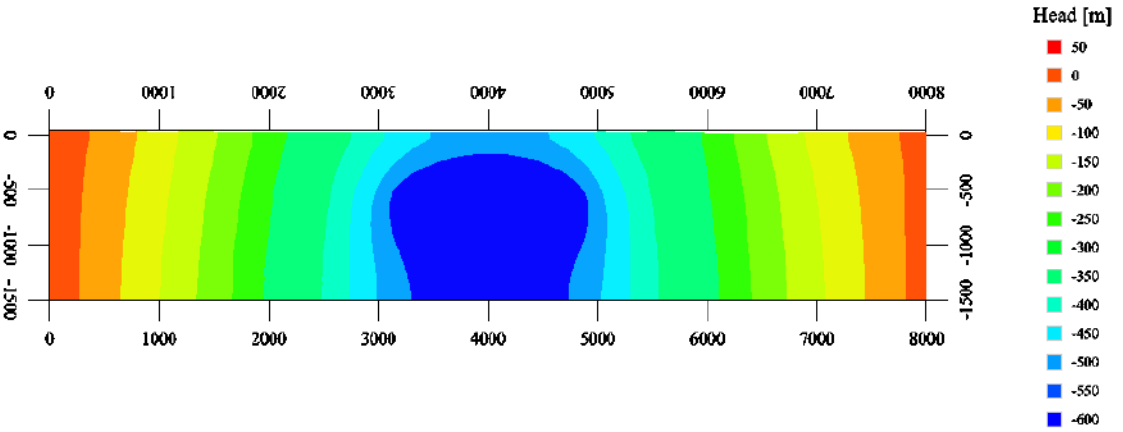

Figure A-5. *Simulation L0_o2 (hydraulic head): phase of desaturation at 100 a (recharge).*

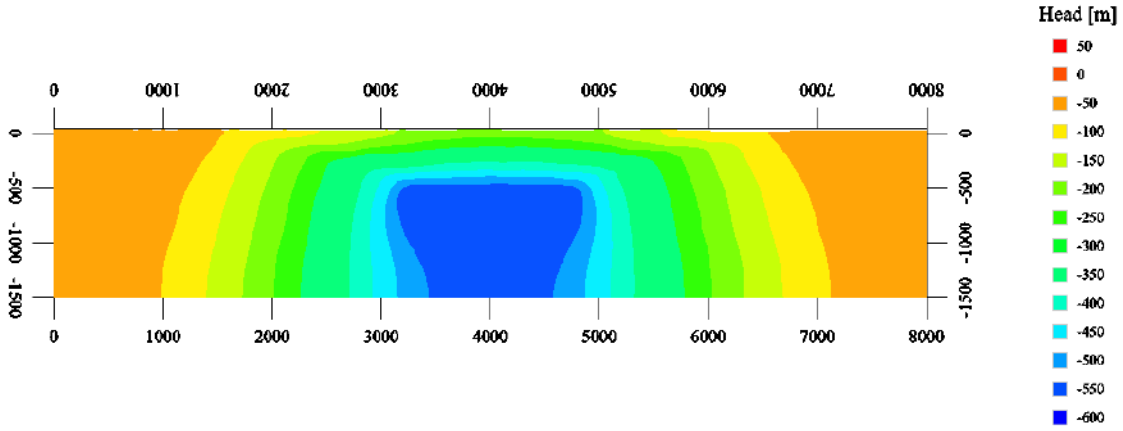

Figure A-6. *Simulation L0_o3 (hydraulic head): phase of desaturation at 100 a (free surface).*

Table A-3. Mass balance: desaturation phase at 100 a.

Simulation	Surface (recharge) (m^3/s)	Surface (exfiltration) (m^3/s)	Lateral (m^3/s)	Surface + lateral (m^3/s)	Repository (m^3/s)
L0_o1	–	–	–	$3.562 \cdot 10^{-5}$	**$-3.563 \cdot 10^{-5}$**
L0_o1_F	–	–	–	$2.536 \cdot 10^{-4}$	$-2.536 \cdot 10^{-4}$
L0_o2	$6.404 \cdot 10^{-6}$	–	$4.876 \cdot 10^{-6}$	–	$-1.129 \cdot 10^{-5}$
L0_o3	$6.222 \cdot 10^{-6}$	$-2.797 \cdot 10^{-7}$	$1.964 \cdot 10^{-6}$	–	$-7.915 \cdot 10^{-6}$
L0_o3_F	$6.222 \cdot 10^{-6}$	$-2.202 \cdot 10^{-7}$	$2.139 \cdot 10^{-6}$	–	$-8.131 \cdot 10^{-6}$

In terms of flow field, simulation L0_o3 integrates the general characteristics of the other two cases. Therefore, simulation L0_o3 with a free surface corresponds to a more realistic flow field than simulations L0_o1 and L0_o2 which represent end members for the flow field.

For simulations L0_o1_F and L0_o3_F, a fracture zone intersecting the repository (with a hydraulic conductivity of 10^{-5} m/s) was introduced in the model (cf Figure 4-14). The results (see Table A-3) show that for the boundary condition with a fixed hydraulic potential (option 1), the fracture zone increases the flow rate to the repository by a factor of 10. This effect is strongly reduced when free surface boundary conditions are applied because the available quantity of water is constrained by the recharge.

The pressure fields of simulations L0_o1, L0_o2 and L0_o3 (see Figure A-7, Figure A-8 and Figure A-9) are of interest with respect to near-surface effects. In particular, knowledge of the size of zones with negative pressure conditions is essential for environmental impact assessments for the phase of repository operation. The results show that for boundary conditions with fixed potential (simulation L0_o1) no desaturation effects can occur; i.e. sufficient water is always provided within the model when applying this type of boundary condition. The near-surface effects can not be evaluated using boundary conditions with fixed potential.

For simulations L0_o2 and L0_o3, zones with negative pressure are obtained. The near-surface impact associated with free surface boundary conditions (simulation L0_o3) is of lesser extent than that associated with recharge boundary conditions (simulation L0_02). This difference is caused by the reduction in hydraulic conductivity (factor 10) which affects the unsaturated zone when performing simulations under free surface conditions. Therefore, this type of boundary condition (option 3) is more adequate for near-surface assessment.

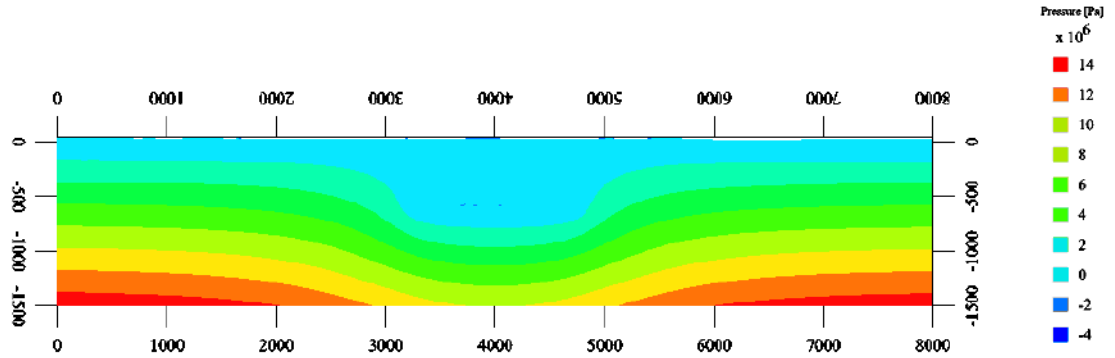

Figure A-7. *Simulation L0_o1 (pressure): phase of desaturation at 100 a (fixed head).*

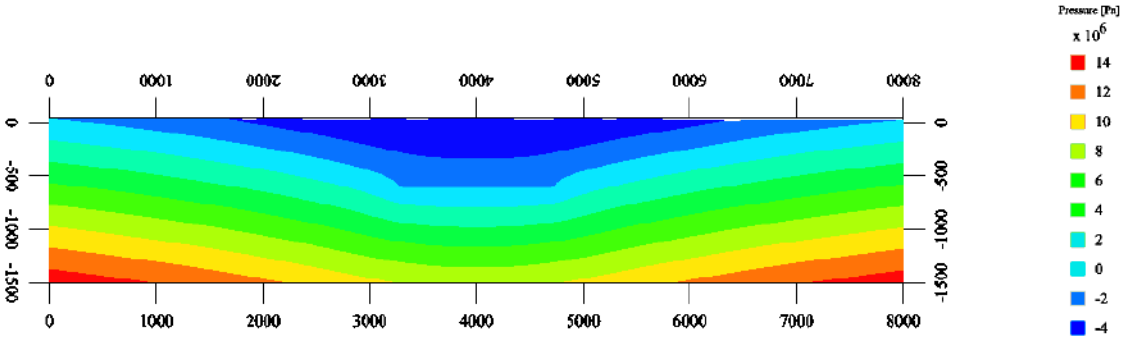

Figure A-8. *Simulation L0_o2 (pressure): phase of desaturation at 100 a (recharge).*

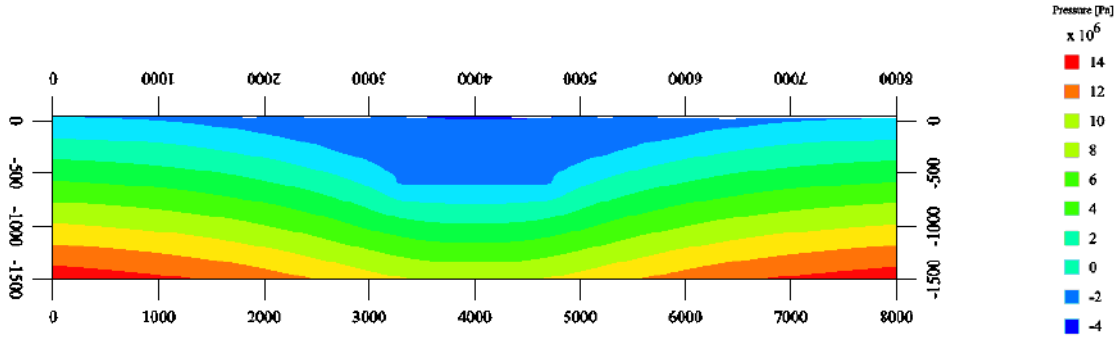

Figure A-9. *Simulation L0_o3 (pressure): phase of desaturation at 100 a (free surface).*

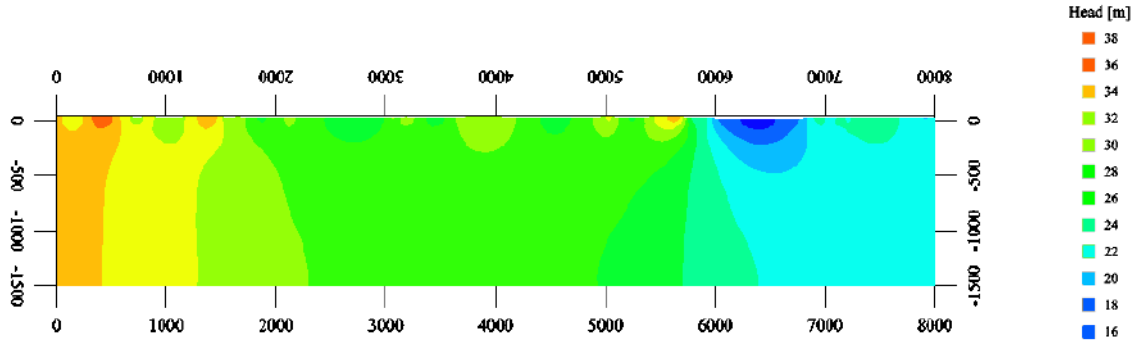

Figure A-10. *Simulation L0_o1 (hydraulic head): phase of resaturation 35 a after repository closure (fixed head).*

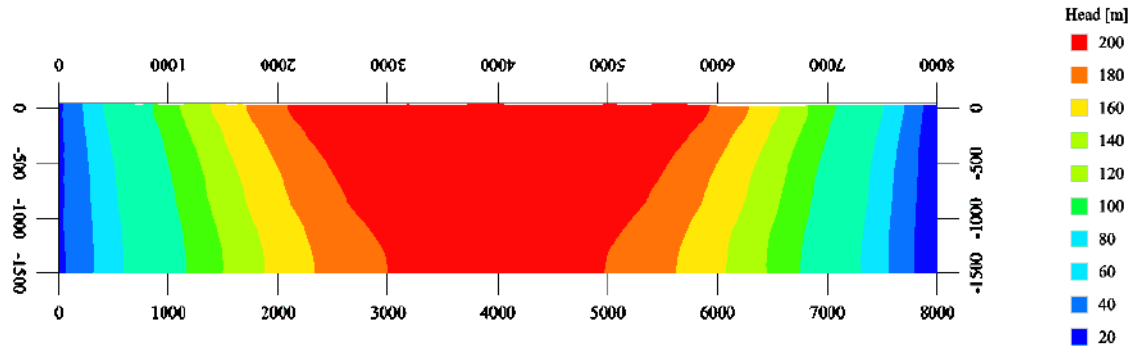

Figure A-11. *Simulation L0_o2 (hydraulic head): phase of resaturation 35 a after repository closure (recharge).*

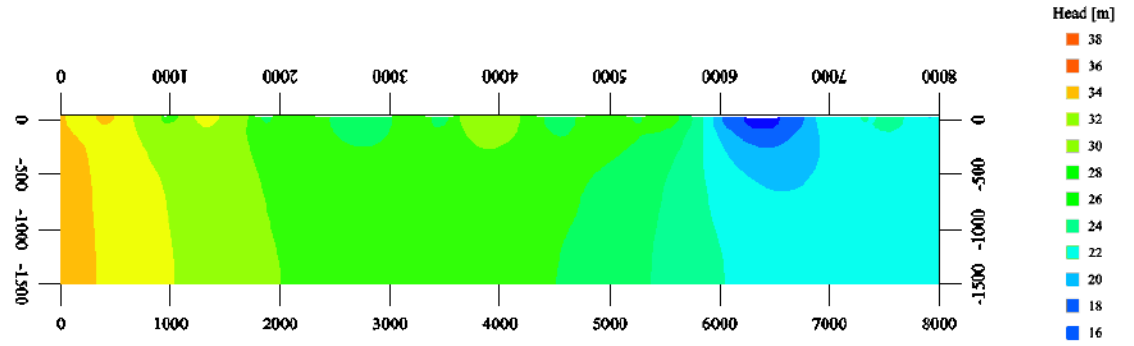

Figure A-12. *Simulation L0_o3 (hydraulic head): phase of resaturation 35 a after repository closure (free surface).*

For the resaturation phase, the results for simulations L0_o1 and L0_o3 show that 35 a after repository closure, the influence of the repository is no longer observable. For simulation L0_o2, the recharge boundary condition becomes dominant and leads to the same type of unrealistic flow field observed for the calculation of initial conditions (cf Figure A-2).

Final remarks

Based on the 2D scoping calculations, it appears that free surface boundary conditions are likely to produce more realistic results in terms of repository impact at repository level as well as at the near surface (see Table A-4).

Table A-4. Pros and cons of boundary conditions.

Boundary condition	Desaturation effects	Time scale for resaturation	Maximum concentration	Flow rate in repository	Environmental impact
Fixed head	None: confined aquifer	Underestimation	Potential underestimation: more freshwater	Overestimation (recharge is too large)	Not adapted
Recharge	Limited effect (confined aquifer)	None: unrealistic resaturation phase	Potentially improved estimation	Improved estimation	Overestimation
Free surface	Realistic: unconfined aquifer	Improved estimation	Potentially improved estimation	Realistic estimation	Adapted